Mon. Not. R. Astron. Soc. **000**, 1–?? (2005) Printed 25 July 2014 (MN LATEX style file v2.2)

Formation and evolution of molecular hydrogen in disk galaxies with different masses and Hubble types

Kenji Bekki[1⋆]
[1]*ICRAR M468 The University of Western Australia 35 Stirling Hwy, Crawley Western Australia 6009, Australia*

arXiv:1407.6468v1 [astro-ph.GA] 24 Jul 2014

Accepted, Received 2005 February 20; in original form

ABSTRACT

We investigate the physical properties of molecular hydrogen (H_2) in isolated and interacting disk galaxies with different masses and Hubble types by using chemodynamical simulations with H_2 formation on dust grains and dust growth and destruction in interstellar medium (ISM). We particularly focus on the dependences of H_2 gas mass fractions (f_{H_2}), spatial distributions of H I and H_2, and local H_2-scaling relations on initial halo masses (M_h), baryonic fractions (f_{bary}), gas mass fractions (f_g), and Hubble types. The principal results are as follows. The final f_{H_2} can be larger in disk galaxies with higher M_h, f_{bary}, and f_g. Some low-mass disk models with M_h smaller than $10^{10}M_\odot$ show extremely low f_{H_2} and thus no/little star formation, even if initial f_g is quite large (> 0.9). Big galactic bulges can severely suppress the formation of H_2 from H I on dust grains whereas strong stellar bars can not only enhance f_{H_2} but also be responsible for the formation of H_2-dominated central rings. The projected radial distributions of H_2 are significantly more compact than those of H I and the simulated radial profiles of H_2-to-H I-ratios (R_{mol}) follow roughly $R^{-1.5}$ in MW-type disk models. Galaxy interaction can significantly increase f_{H_2} and total H_2 mass in disk galaxies. The local surface mass densities of H_2 can be correlated with those of dust in a galaxy. The observed correlation between R_{mol} and gas pressure ($R_{mol} \propto P_g^{0.92}$) can be well reproduced in the simulated disk galaxies.

Key words: ISM: molecules – galaxies:ISM – galaxies:evolution – infrared:galaxies – stars:formation

1 INTRODUCTION

Formation and evolution processes of molecular hydrogen (H_2) and interstellar dust in galaxies can be strongly coupled, because the surface of dust grains can be the major formation sites of H_2 (e.g., Gould & Salpeter 1963; Hollenbach & Salpeter 1971). Dust has long been considered to play decisive roles in several aspects of star and galaxy formation, such as radiative cooling processes in star-forming clouds (e.g., Herbst 2001) and the formation of metal-poor low-mass stars in the early universe (e.g., Schneider & Omukai 2010). Likewise, H_2 is an essential element in giant molecular clouds where star formation is ongoing (e.g., Blitz et al. 2007; Fukui & Kawamura 2010) and its physical properties (e.g., mass densities) are key parameters for the observed star-formation laws in galaxies (e.g., Bigiel et al. 2008; Leroy et al. 2008). Thus, the better understanding of the formation and evolution processes of *both* dust and H_2 in ISM can lead to the deeper understanding of galaxy formation and evolution in general.

Physical properties of H_2 have long been investigated for galaxies with different Hubble types (e.g., Young & Scoville 1991, YS91; Boselli et al. 2014), in different environments (e.g., Leon et al. 1998; Wilson et al. 2009), and at different redshifts (e.g., Daddi eta l. 2010; Tacconi et al. 2010; Bauermeister et al. 2013), and their origins have not been clarified yet. Recent extensive observational studies on H I and H_2 properties of galaxies and their correlations of galaxy parameters for a large number of galaxy samples have provided valuable information on scaling relations of gas and stars and thus new constraints on galaxy formation and evolution. (e.g., Catinella et al. 2010; Saintonge et al. 2011). Resolved structures and kinematics of giant molecular clouds (GMCs) in nearby galaxies such as M31, M33, and the Large Magellanic Cloud (LMC) have enabled astronomers to reveal the physical factors for the conversion from H I to H_2 and the possible typical lifetime of GMCs in galaxies (e.g., Blitz et al. 2007; Fukui & Kawamura 2010).

In spite of these observational progresses, a number of

⋆ E-mail: bekki@cyllene.uwa.edu.au

key long-standing problems on H_2 properties of galaxy have not been resolved yet. Among them is the origin of the diverse H_2 properties along the Hubble sequence (e.g., YS91). It is well known that the mass-ratio of H_2 to H I (referred to as $R_{\rm mol}$) is quite diverse (more than two orders of magnitudes) for a given Hubble type and it is systematically higher in early-type disk galaxies (YS91). This diverse H_2 properties along the Hubble sequence has been confirmed in the latest observations with a larger number of galaxy samples (e.g., Boselli et al. 2014). It is theoretically unclear what global galaxy parameters (e.g., bulge-to-disk-ratios) can determine the observed H_2-to-H I-ratios ($R_{\rm mol}$) in galaxies.

Furthermore, one of other unresolved problems is related to the observed radial distributions of H_2 in galaxies and their correlations with stellar parameters of galaxies (e.g., Blitz et al. 2007). Wong & Blitz (2002) showed that the ratio of H_2 to H I surface density in a galaxy depends on the projected distance (R) from the galactic center such that it can be best fit to $R^{-1.5}$ (or R^{-1}, see their Fig. 14). Some early-type spirals (e.g., M31) are observed to have intriguing ring-like structures (e.g., YS91). Recent observations have revealed that the mass-ratio of H_2 to stars ($M_{\rm H_2}/M_*$) is quite different between galaxies with different Hubble types and even within a same type (e.g., Boselli et al. 2014). These observations have not been explained clearly by previous theoretical studies of galaxy formation and evolution, though they would have some profound implications on galaxy formation.

Recent significant progresses in observational studies of H_2 properties of galaxies with different types at different z appear to have triggered extensive theoretical and numerical studies of of H_2 formation in galaxies. For example, recent numerical simulations of galaxy formation and evolution have incorporated the conversion of H_2 formation from H I on dust grains (e.g., Pelupessy et al. 2006, P06; Robertson & Kravtsov 2008, Gnedin et al. 2009; Christensen et al. 2012; Kuhlen et al. 2012; Thompson et al. 2014). Recent semi-analytic models of galaxy formation (e.g., Fu et al. 2010; Lagos et al. 2012) adopted the H_2 formation model dependent gaseous metallicities and densities proposed by Krumholz, McKee & Tumlinson (2009) and thereby investigated the time evolution of H_2 contents in galaxies.

However, these previous numerical studies of galaxy formation and evolution with H_2 formation have not incorporated the evolution of dust (e.g., abundances and masses) explicitly in their models, and accordingly could not discuss the importance of the *joint* evolution of dust and H_2. It is ideal for any theoretical studies of H_2 formation in galaxies to include the formation and evolution processes of both dust and H_2 in a self-consistent manner, because their evolution can be strongly coupled through star formation. Given that recent observational studies have revealed a number of important correlations between dust and H_2 properties in galaxies (e.g., Corbelli et al. 2012), it would be essential for theoretical studies of H_2 formation in galaxies to incorporate a model for the formation and evolution of dust in ISM.

Our previous studies constructed a new chemodynamical model that includes both the H_2 formation on dust grains and the formation and destruction of dust in ISM in a self-consistent manner (Bekki 2013a, 2014; B13a and B14, respectively, Yozin & Bekki 2014a). They therefore could discuss the time evolution of dust and H_2 properties in galaxies at their formation epochs. However, they did not discuss how the physical properties of H_2 in galaxies can possibly depend on their global parameters such as their total masses and Hubble types. Therefore, the following three questions are unresolved: (i) what can drive the observed diversity in H_2 properties between different galaxies, (ii) whether and how dust can play a role in controlling H_2 properties of galaxies, and (iii) what is responsible for the observed H_2-dust correlations in galaxies.

The purpose of this paper are two-fold as follows. First, we investigate whether the adopted model of H_2 formation self-consistently including dust evolution can explain the observed fundamental properties of H_2 in galaxies. In this first investigation, we focus particularly on the observed correlations between mass-ratios of H_2 to H I and other galaxy parameters (e.g., Wong & Blitz 2002; Blitz & Rosolowsy 2006, Blitz et al. 2007). Second, we investigate how the physical properties of H_2 in galaxies depend on the total halo masses ($M_{\rm h}$), baryonic mass fractions ($f_{\rm bary}$), gas mass fractions ($f_{\rm g}$), Hubble types (e.g., bulge-to-disk-ratios, $f_{\rm b}$), and the formation redshifts of galaxies by using mainly isolated models of disk and dwarf galaxies. We also try to understand how galaxy interaction can influence the time evolution of global H_2 properties of galaxies in this second investigation.

The plan of the paper is as follows. We describe some details of the chemodynamical model with the formation and evolution of dust and H_2 adopted by the present study in §2. We present the numerical results on the physical correlations between H_2 properties and galaxy parameters (e.g., masses) in disk galaxies in §3. In this section, we also discuss the dependences of the results on the adopted model parameters. In §4, we discuss the latest observational results on H_2 properties of galaxies and provides some implications of some key results derived in this paper. We summarize our conclusions in §5.

In the present, we do not discuss the latest results from *ALMA* (Atacama Large Millimeter Array), such as the molecular outflow driven by AGN (e.g., Combes et al. 2014) and total ISM masses probed by dust emission in 107 galaxies from $z = 0.2$ to $z = 2.5$ (Scoville et al. 2014). These new observational results will be addressed by our future works with a more sophisticated chemodynamical model with H_2 formation.

2 THE MODEL

2.1 A new simulation code

We adopt our new simulation code recently developed in our previous works (B13a and B14) in order to investigate spatial and temporal variations of H_2 in disk galaxies with different masses and Hubble-types. The adopted code can be run on GPU-based machines (clusters), where gravitational calculations can be done on GPUs whereas other calculations (e.g., star formation and hydrodynamics) can be done on CPUs. The code adopts the smoothed-particle hydrodynamics (SPH) method for following the time evolution of gas dynamics in galaxies.

The present simulations include the formation of dust grains in the stellar winds of supernovae (SNe) and asymptotic giant branch (AGB) stars, the time evolution of interstellar radiation field (ISRF), the growth and destruction

Table 1. A list of physical processes implemented in the present simulated code.

Physical effects	Inclusion or not [a]	Specifications
H_2 formation on dust grains	◯	H_2 formation efficiency dependent on D and $ISRF$
H_2 photodissociation by ISRF	◯	ISRF locally defined for each gas particle
Dust formation	◯	Formation in SNe and AGB stars
Dust growth	◯	Dust growth timescale dependent on gas properties
Dust destruction	◯	Destruction by SNe (but not by hot plasma etc)
Size evolution of dust	×	
Size-dependence on dust composition	×	
Stellar radiation pressure on dust	×	
Gas-dust hydrodynamical coupling	×	
Star formation	◯	H_2-dependent recipe
SN feedback effects	◯	Both SNII and prompt SNIa are included.
AGN feedback effects	×	
Growth of SMBHs	×	
Chemical evolution	◯	11 elements (e.g., C, N, and O)
Chemical enrichment by AGB ejecta	◯	
Metallicity-dependent radiative cooling	◯	Only for $T_g > 10^4$ K (no H_2-dependent cooling for low T_g)
Time-dependent IMF	×	A fixed canonical IMF is adopted.

[a] ◯ and × in the second column mean inclusion and non-inclusion of the listed physical effect, respectively

processes of dust in the interstellar medium (ISM), the H_2 formation on dust grains, and the H_2 photo-dissociation due to far ultra-violet (FUV) light in a self-consistent manner. Although we can investigate the formation of polycyclic aromatic hydrocarbon (PAH) dust in carbon-rich AGB stars and the time evolution of dust by using the simulation code, we do not extensively investigate the dust properties in the present study. Instead, we briefly discuss the possible physical correlations between dust and H_2 properties in disk galaxies.

The new simulation code does not include the effects of feedback of active galactic nuclei (AGN) on ISM and the growth of supermassive black holes (SMBHs) in galaxies so that we can not investigate how the feedback can change the spatial distributions and mass budgets of dust and H_2 in galaxies. Although it is an important issue whether and how the AGN feedback effects can influence the dust properties of ISM and thus the H_2 contents, we will discuss this in our future papers. The new code allows us to choose whether some physical effects (e.g., dust formation etc) are included or excluded (i.e., 'switched on or off') so that we can investigate how the physical effects are important in the evolution of gas and stars in galaxies. Accordingly, we summarize the physical effects that are included in the present study in Table 1 for clarity.

Since the major formation site of H_2 in ISM is the surface of dust grains, it is crucial for any theoretical study on H_2 evolution of galaxies to properly investigate the time evolution of dust abundances in disk galaxies. Given that both observational and theoretical studies have shown that dust-to-metal-ratios can be diverse (e.g., Hirashita 1999; Galametz et al. 2011), we need to refrain from deriving dust abundances from metallicities by assuming constant dust-to-metal-ratios. The present code indeed enables us to investigate the time evolution of different dust components in galaxies so that we can more properly predict the time evolution of H_2 in galaxies. We mainly focus on isolated disk galaxies composed of dark matter halo, stellar disk, stellar bulge, and gaseous disk: Some new results on H_2 properties in forming galaxies at high redshifts (z) are discussed in B14. Since the details of the physical models for the formation and evolution of dust and H_2 are given in B13 and B14, we briefly describe the models in the present paper.

2.2 A disk galaxy

2.2.1 Structure and kinematics

The total masses of dark matter halo, stellar disk, gas disk, and bulge of a disk galaxy are denoted as M_h, M_s, M_g, and M_b, respectively. The total disk mass (gas + stars) and gas mass fraction are denoted as M_d and f_g, respectively, for convenience. The mass ratio of the disk ($M_s + M_g$) to the dark matter halo (M_h) in a disk galaxy is a 'baryonic mass fraction' and denoted as f_{bary}. The bulge-to-disk-ratio is defined as M_b/M_s and represented by a parameter f_b. The four key parameters in the present study are M_h, f_g, f_{bary}, and f_b.

In order to describe the initial density profile of dark matter halo in a disk galaxy, we adopt the density distribution of the NFW halo (Navarro, Frenk & White 1996) suggested from CDM simulations:

$$\rho(r) = \frac{\rho_0}{(r/r_s)(1+r/r_s)^2}, \quad (1)$$

where r, ρ_0, and r_s are the spherical radius, the characteristic density of a dark halo, and the scale length of the halo, respectively. The c-parameter ($c = r_{vir}/r_s$, where r_{vir} is the virial radius of a dark matter halo) and r_{vir} are chosen appropriately for a given dark halo mass (M_{dm}) by using the $c - M_h$ relation for $z = 0$ and 2 predicted by recent cosmological simulations (e.g., Neto et al. 2007; Muñoz-Cuartas et al. 2011).

The bulge of a disk galaxy has a size of R_b and a scale-length of $R_{0,b}$ and is represented by the Hernquist density profile. The bulge is assumed to have isotropic velocity dispersion and the radial velocity dispersion is given according to the Jeans equation for a spherical system. The bulge-to-disk ratio ($f_b = M_b/M_d$) of a disk galaxy is a free parameter ranging from 0 (pure disk galaxy) to 4

Table 2. A brief summary for the values of key model parameters.

Model no	$M_{\rm h}$ [a]	c [b]	$M_{\rm d}$ [c]	$R_{\rm d}$ [d]	$f_{\rm g}$ [e]	$f_{\rm bary}$ [f]	$f_{\rm b}$ [g]	[Fe/H]$_0$ [h]	z [i]	Interaction [j]	Comments
M1	10^{12}	10.0	6.6×10^{10}	17.5	0.09	0.066	0.17	0.0	0	×	Fiducial MW-type
M2	10^{12}	10.0	6.6×10^{10}	17.5	0.05	0.066	0.17	0.06	0	×	gas-poor
M3	10^{12}	10.0	6.6×10^{10}	17.5	0.27	0.066	0.17	−0.16	0	×	gas-rich
M4	10^{12}	10.0	3.3×10^{10}	17.5	0.09	0.033	0.17	0.0	0	×	Lower baryonic fraction
M5	10^{12}	10.0	1.7×10^{10}	17.5	0.09	0.017	0.17	0.0	0	×	
M6	10^{12}	10.0	1.7×10^{10}	17.5	0.55	0.033	0.17	−0.44	0	×	
M7	10^{12}	10.0	6.6×10^{10}	17.5	0.09	0.066	0.0	0.0	0	×	
M8	10^{12}	10.0	6.6×10^{10}	17.5	0.09	0.066	1.0	0.0	0	×	
M9	10^{12}	10.0	6.6×10^{10}	17.5	0.09	0.066	2.0	0.0	0	×	
M11	10^{12}	10.0	1.8×10^{10}	17.5	0.33	0.018	0.17	0.0	0	×	
M12	10^{12}	10.0	1.8×10^{10}	17.5	0.33	0.018	4.0	0.0	0	×	
M13	10^{12}	10.0	6.6×10^{10}	43.8	0.09	0.066	0.17	0.0	0	×	LSB model
M14	10^{12}	4.5	6.6×10^{10}	11.3	0.09	0.066	0.17	0.0	2	×	High-z disk
M15	10^{12}	4.5	3.3×10^{10}	11.3	0.55	0.033	0.17	−0.44	2	×	High-z disk
M16	10^{12}	10.0	6.6×10^{10}	17.5	0.09	0.066	0.17	0.0	0	◯	Prograde interaction
M17	10^{12}	10.0	6.6×10^{10}	17.5	0.09	0.066	0.17	0.0	0	◯	Retrograde interaction
M18	10^{12}	10.0	6.6×10^{10}	17.5	0.09	0.066	0.17	0.0	0	◯	Highly inclined disk
M19	10^{12}	10.0	6.6×10^{10}	17.5	0.09	0.066	0.17	0.0	0	◯	More distance encounter
M20	10^{11}	12.6	6.6×10^{9}	5.5	0.09	0.066	0.0	−0.46	0	×	Less massive disk
M21	10^{11}	12.6	6.6×10^{9}	5.5	0.27	0.066	0.0	−0.62	0	×	
M22	10^{11}	12.6	6.6×10^{9}	5.5	0.55	0.066	0.0	−0.90	0	×	
M23	10^{11}	12.6	6.6×10^{9}	5.5	0.27	0.033	0.0	−0.62	0	×	
M24	10^{11}	4.9	3.3×10^{9}	3.5	0.55	0.033	0.0	−0.90	2	×	
M25	10^{10}	16.0	6.6×10^{8}	1.8	0.09	0.066	0.0	−0.92	0	×	Dwarf disk
M26	10^{10}	16.0	6.6×10^{8}	1.8	0.27	0.066	0.0	−1.08	0	×	
M27	10^{10}	16.0	6.6×10^{8}	1.8	0.55	0.066	0.0	−1.36	0	×	
M28	10^{10}	16.0	3.3×10^{8}	1.8	0.55	0.033	0.0	−1.36	0	×	
M29	10^{10}	16.0	1.3×10^{8}	1.8	0.55	0.013	0.0	−1.36	0	×	
M30	10^{10}	16.0	6.6×10^{7}	1.8	0.55	0.007	0.0	−1.36	0	×	
M31	3×10^{9}	17.8	9.9×10^{7}	1.0	0.55	0.033	0.0	−1.60	0	×	Low-mass dwarf
M32	3×10^{9}	17.8	9.9×10^{6}	1.0	0.98	0.003	0.0	−2.70	0	×	Very gas-rich dwarf
M33	10^{9}	20.0	1.3×10^{7}	0.6	0.55	0.013	0.0	−1.50	0	×	The least massive dwarf
M34	10^{9}	20.0	7.2×10^{6}	0.6	0.92	0.007	0.0	−2.90	0	×	

[a] The total mass of dark matter halo of a disk galaxy in units of $\rm M_\odot$.
[b] The 'c' parameter of the adopted NFW profile for dark matter halo in a galaxy.
[c] The total disk mass (gas +stars) of a disk galaxy in units of $\rm M_\odot$.
[d] The stellar disk size of a disk galaxy in units of kpc.
[e] The gas mass fraction ($M_{\rm g}/M_{\rm d}$) in a disk galaxy.
[f] The baryonic mass fraction ($M_{\rm d}/M_{\rm h}$) in a disk galaxy.
[g] The bulge mass fraction ($M_{\rm b}/M_{\rm d}$) in a disk galaxy.
[h] The initial mean gas-phase metallicity for the disk of a galaxy.
[i] The virialization redshift z (or formation redshift) of a dark halo and this z is used to estimate $r_{\rm vir}$ and c.
[j] ◯ and × mean inclusion and non-inclusion of galaxy interaction, respectively.

(bulge-dominated). The 'MW-type' models are those with $f_{\rm b}=0.17$ and $R_{\rm b}=0.2R_{\rm s}$, where $R_{\rm s}$ is the stellar disk size of a galaxy. We adopt the mass-size scaling relation of $R_{\rm b}=C_{\rm b}M_{\rm b}^{0.5}$ for bulges so that we can determine $R_{\rm b}$ for a given $M_{\rm b}$. The value of $C_{\rm b}$ is determined so that $R_{\rm b}$ can be 3.5 kpc for $M_{\rm b}=10^{10}\rm M_\odot$ (corresponding to the mass and size of the MW's bulge).

The radial (R) and vertical (Z) density profiles of the stellar disk are assumed to be proportional to $\exp(-R/R_0)$ with scale length $R_0=0.2R_{\rm s}$ and to $\rm sech^2(Z/Z_0)$ with scale length $Z_0=0.04R_{\rm s}$, respectively. The gas disk with a size $R_{\rm g}=2R_{\rm s}$ has the radial and vertical scale lengths of $0.2R_{\rm g}$ and $0.02R_{\rm g}$, respectively. In the present model for the MW-type, the exponential disk has $R_{\rm s}=17.5$ kpc and $R_{\rm g}=35$ kpc. In addition to the rotational velocity caused by the gravitational field of disk, bulge, and dark halo components, the initial radial and azimuthal velocity dispersions are assigned to the disc component according to the epicyclic theory with Toomre's parameter $Q=1.5$. The vertical velocity dispersion at a given radius is set to be 0.5 times as large as the radial velocity dispersion at that point.

The total numbers of particles used for dark matter halo ($N_{\rm dm}$), stellar disk ($N_{\rm s}$), and gaseous disk ($N_{\rm g}$) in a simulation are 700000, 200000, and 100000 respectively. The total number of particle for bulge is $f_{\rm b}N_{\rm s}$, which means that $N_{\rm b}=33400$ for the MW-type disk galaxy model with $f_{\rm b}=0.167$ and 400000 for the big bulge model with $f_{\rm b}=2$. Therefore, the total number of particles is $N=1033400$ for the fiducial MW-type model and $N=1400000$ for the big bulge model. The gravitational softening length for each component is determined by the number of particle used for

Table 3. Description of the basic parameter values for the models of star formation, dust, and chemical evolution.

Parameters	Adopted values	The standard value adopted in most models
τ_0 [a]	0.1, 0.2, 0.4, 2 Gyr	0.2 Gyr
$\beta_{\rm d}$ [b]	1, 2, 4	2
$f_{\rm dust}$ [c]	0.1, 0.4	0.4
Dust yield	B13a (fixed)	–
Chemical yield	T95 for SN, VG97 for AGB	–
α [d]	0, −0.04	0
$\rho_{\rm th}$ [e]	1 $\rm cm^{-3}$ (fixed)	–
IMF	Kroupa (fixed)	–

[a] The dust growth timescale for a gas density of 1 atom $\rm cm^{-3}$ for the adopted variable dust accretion model.
[b] The ratio of dust destruction timescale of a gas disk.
[c] The initial dust-to-metal-ratio to dust growth timescale.
[d] The initial metallicity gradient (of the gas disk) in units of dex $\rm kpc^{-1}$.
[e] $\rho_{\rm th}$ is the threshold H_2 gas density for star formation for each gas particle.

each component and by the size of the distribution (e.g., $R_{\rm s}$ and $r_{\rm vir}$) and the value is described later.

2.2.2 Gas-phase metallicity and its radial gradient

Observations have shown that (i) there is a mass-metallicity relation in disk galaxies (e.g., Tremonti et al. 2004) and (ii) most of disk galaxies show negative metallicity gradients (i.e., higher metallicity in inner regions) with the slopes being different in different galaxies (e.g., Zaritsky et al. 1994). We therefore determine the initial mean metallicity of the gas disk in a galaxy according to the observe mass-metallicity relation for the adopted total halo mass ($M_{\rm h}$) and gas mass fraction for the galaxy. For example, a MW-type disk galaxy with $M_{\rm h} = 10^{12}{\rm M}_\odot$ ($M_{\rm s} = 6 \times 10^{10}{\rm M}_\odot$) and $f_{\rm g} = 0.09$ (corresponding to the fiducial model later described) can have [Fe/H]=0.

The gas-phase metallicity of each (gaseous and stellar) particle is given according to its initial position: at $r = R$, where r (R) is the projected distance (in units of kpc) from the center of the disk, the metallicity of the star is given as:

$$[{\rm Fe/H}]_{\rm r=R} = [{\rm Fe/H}]_{\rm d,r=0} + \alpha \times {\rm R}. \quad (2)$$

where α is the slope of the metallicity gradient in units of dex $\rm kpc^{-1}$. Since the present results on global properties of H_2 do not depend on α, we mainly show the results of the models with $\alpha = 0$. We however discuss briefly how the present results can change if we adopt a steeper metallicity gradient of $\alpha = -0.04$, which is the observed value of our Milky Way (e.g., Andrievsky et al. 2004).

2.2.3 Low-z vs high-z disks

Since we mainly investigate H_2 properties of disk galaxies at $z = 0$, we construct the disk model by using the $c - M_{\rm h}$ relation for dark matter halos at $z = 0$ (e.g., Neto et al. 2007; Muñoz-Cuartas et al. 2011). We however investigate a number of disk models that can represent disk galaxies at high z by using the $c-M_{\rm h}$ relation dependent on z (Muñoz-Cuartas et al. 2011). In constructing the disk models at high z, we consider the following two theoretical and observational results. First, the mean density of a dark matter halo ($\rho_{\rm dm}$) with $M_{\rm h}$ at z is $(1 + z)^3$ times higher than that (of a dark matter halo with the same $M_{\rm h}$) at $z = 0$ ($\rho_{\rm dm,0}$). Second, the stellar disk size of a galaxy at z ($R_{\rm s}$) is $(1+z)^{-0.4}$ times larger than that at $z = 0$ ($R_{\rm s,0}$). Therefore the mean density of a dark matter halo in a disk galaxy at $z = 0$ is as follows;

$$\rho_{\rm dm}(z) = \rho_{\rm dm,0}(1 + z)^3, \quad (3)$$

where $r_{\rm vir}(z) \propto \rho_{\rm dm}^{-1/3}$ for a given $M_{\rm h}$. The stellar disk size is given as follows:

$$R_{\rm s}(z) = R_{\rm s,0}(1 + z)^{-0.4}, \quad (4)$$

which means that the size ratio of $r_{\rm vir}$ to $R_{\rm s}$ is proportional to $(1+z)^{-0.6}$. For example, c and $r_{\rm vir}$ for a disk galaxy with $M_{\rm h} = 10^{12}{\rm M}_\odot$ at $z = 0$ are 10 and 245kpc, respectively, whereas they are 4.5 and 82 kpc at $z = 2$. The simulated dark matter halos are assumed to have a scaling relation of $r_{\rm vir} \propto M_{\rm h}^{0.5}$ at $z = 0$ and 2.

2.3 Star formation

Since SF can proceed in molecular clouds, we adopt the following 'H_2-dependent' SF recipe (B13a) using molecular gas fraction ($f_{\rm H_2}$) defined for each gas particle in the present study. A gas particle *can be* converted into a new star if (i) the local dynamical time scale is shorter than the sound crossing time scale (mimicking the Jeans instability) , (ii) the local velocity field is identified as being consistent with gravitationally collapsing (i.e., div $\mathbf{v}< 0$), and (iii) the local density exceeds a threshold density for star formation ($\rho_{\rm th}$). We mainly investigate the models with $\rho_{\rm th} = 1$ $\rm cm^{-3}$ in the present study.

A gas particle can be regarded as a 'SF candidate' gas particle if the above three SF conditions (i)-(iii) are satisfied. It could be possible to convert some fraction ($\propto f_{\rm H_2}$) of a SF candidate gas particle into a new star at each time step until the mass of the gas particle becomes very small. However, this SF conversion method can increase dramatically the total number of stellar particles, which becomes

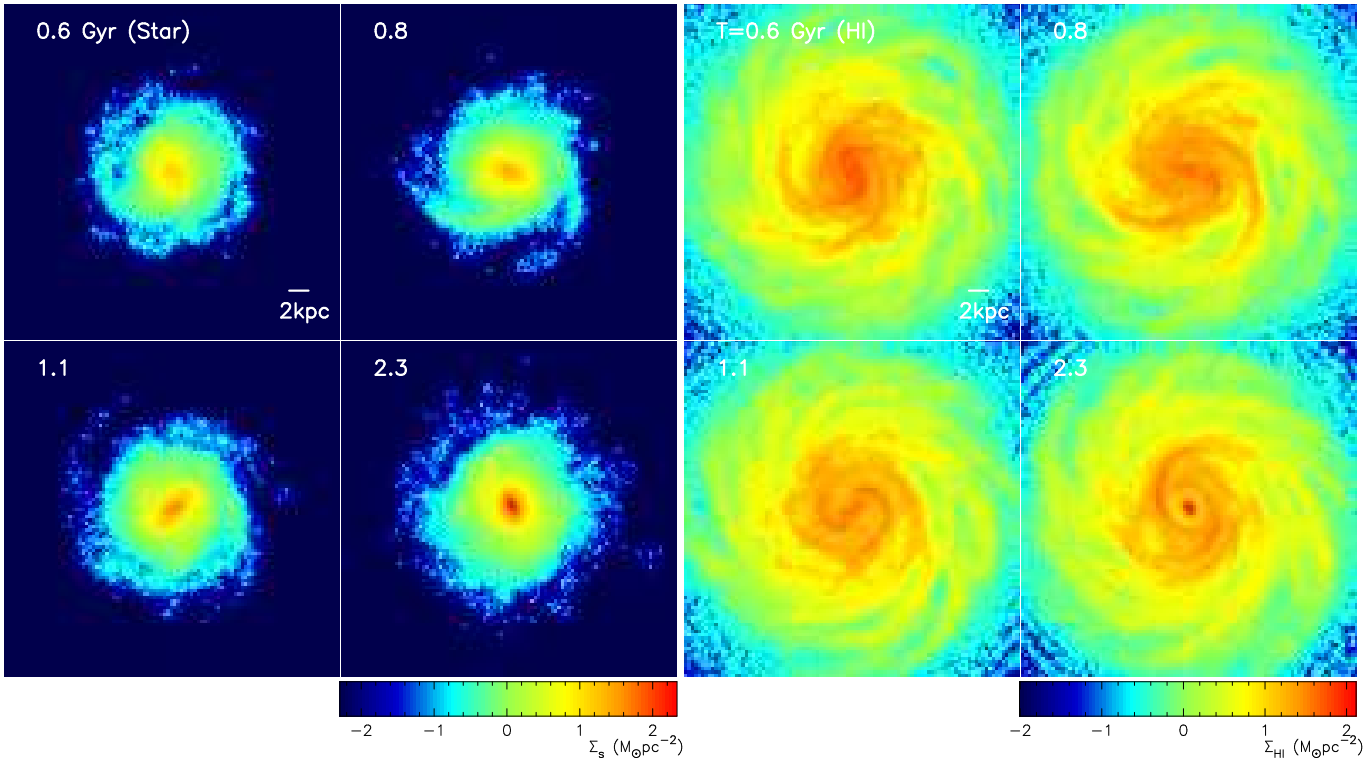

Figure 1. The time evolution of the projected mass densities for stars ($\Sigma_{\rm s}$, left four) and H I (Σ_{HI}, right four) for the fiducial MW-type disk model (M1). The time T, which represents the time that has elapsed since the simulation started, is shown in the upper left corner for each panel. The mass densities are derived from the distributions of particles projected onto the x-y plane of the disk. The projected density fields are smoothed by using a Gaussian kernel with a smoothing length of 875pc.

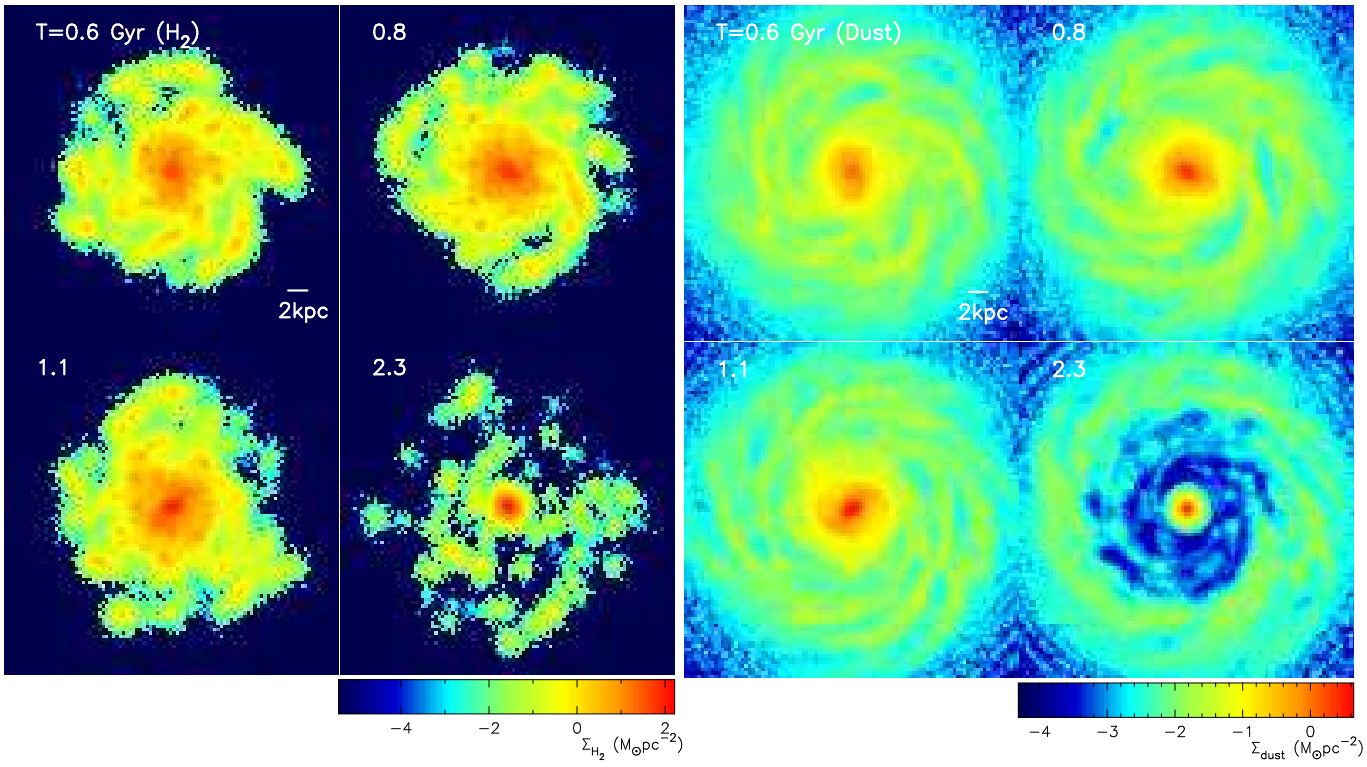

Figure 2. The same as Fig. 1 but for H_2 ($\Sigma_{\rm H_2}$, left four) and for dust ($\Sigma_{\rm dust}$, right four).

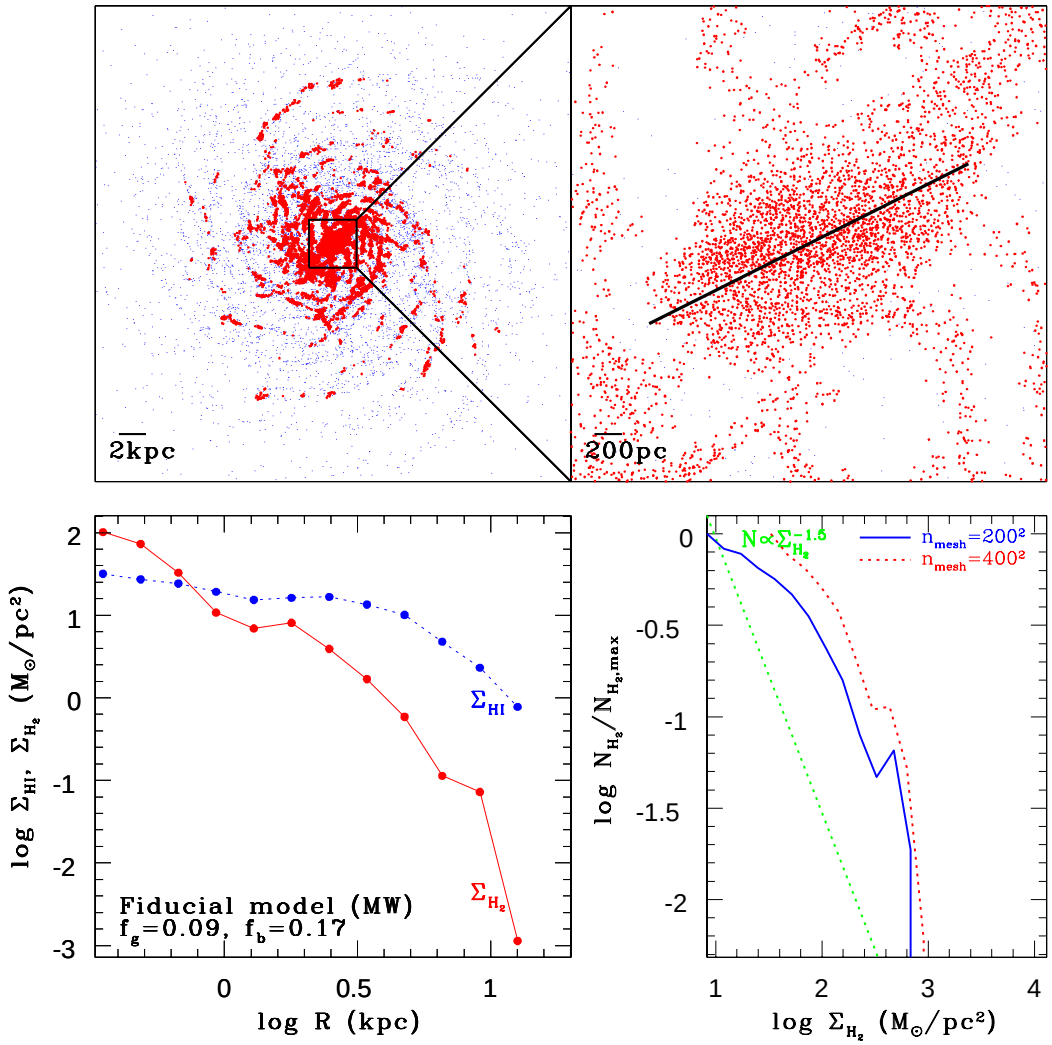

Figure 3. The upper two panels show the distributions of gas with $f_{\rm H_2} < 0.01$ (blue, corresponding to H I-dominated gas) and $f_{\rm H_2} \geqslant 0.01$ (red) projected onto the x-y plane at $T = 1.1$ Gyr in the fiducial MW-type disk model M1. The physical scales in these two panels are different and indicated by a thick bar in each panel. The blue and red dots therefore can represent H I (gas with no/little H_2) and H_2, respectively. The central black thick line in the upper right panel indicates the location of the central stellar bar in this model. Only one in ten particles is shown so that the file size of this figure (in .eps format) can be small enough (yet informative to readers) in these upper panels. The lower left panels shows the (projected) radial distribution of H I ($\Sigma_{\rm HI}$, blue dotted) and H_2 ($\Sigma_{\rm H_2}$, red solid) in the fiducial model. The lower right panel shows the H_2 surface density distribution (H2SDD) normalized by the maximum number of $N_{\rm H_2}$ ($N_{\rm H_2,max}$, where $N_{\rm H_2}$ is the number of meshes with a given H_2 surface density, $\Sigma_{\rm H_2}$) among local regions for $n_{\rm mesh} = 200^2$ (blue solid) and $n_{\rm mesh} = 400^2$ (red dotted) in the fiducial model. The dotted green line indicates $N \propto \Sigma_{\rm H_2}^{-1.5}$, which is similar to the observed molecular cloud mass function (MCMF) of the Galaxy that can be approximated as $N \propto m_{\rm mc}^{-1.5}$, where $m_{\rm mc}$ is the mass of a molecular cloud.

numerically very costly. We therefore adopt the following SF conversion method. A SF candidate i-th gas particle is regarded as having a SF probability ($P_{\rm sf}$);

$$P_{\rm sf} = 1 - \exp(-C_{\rm eff} f_{\rm H_2} \Delta t \rho^{\alpha_{\rm sf}-1}), \quad (5)$$

where $C_{\rm eff}$ corresponds to a star formation efficiency (SFE) in molecular cores and is set to be 1, Δt is the time step width for the gas particle, ρ is the gas density of the particle, and $\alpha_{\rm sf}$ is the power-law slope of the Kennicutt-Schmidt law (SFR$\propto \rho_{\rm g}^{\alpha_{\rm sf}}$; Kennicutt 1998). A reasonable value of $\alpha_{\rm sf} = 1.5$ is adopted in the present study. This SF probability has been already introduced in our early chemodynamical simulations of galaxies (e.g., Bekki & Shioya 1998).

At each time step random numbers ($R_{\rm sf}$; $0 \leqslant R_{\rm sf} \leqslant 1$) are generated and compared with $P_{\rm sf}$. If $R_{\rm sf} < P_{\rm sf}$, then the gas particle can be converted into a new stellar one. In this SF recipe, a gas particle with a higher gas density and thus a shorter SF timescale ($\propto \rho/\dot{\rho} \propto \rho^{1-\alpha_{\rm sf}}$) can be more rapidly converted into a new star owing to the larger $P_{\rm sf}$. Equally, a gas particle with a higher $f_{\rm H_2}$ can be more rapidly converted into a new star. We thus consider that the present SF model is a good approximation for star formation in molecular gas of disk galaxies.

Each SN is assumed to eject the feedback energy ($E_{\rm sn}$) of 10^{51} erg and 90% and 10% of $E_{\rm sn}$ are used for the increase of thermal energy ('thermal feedback') and random motion

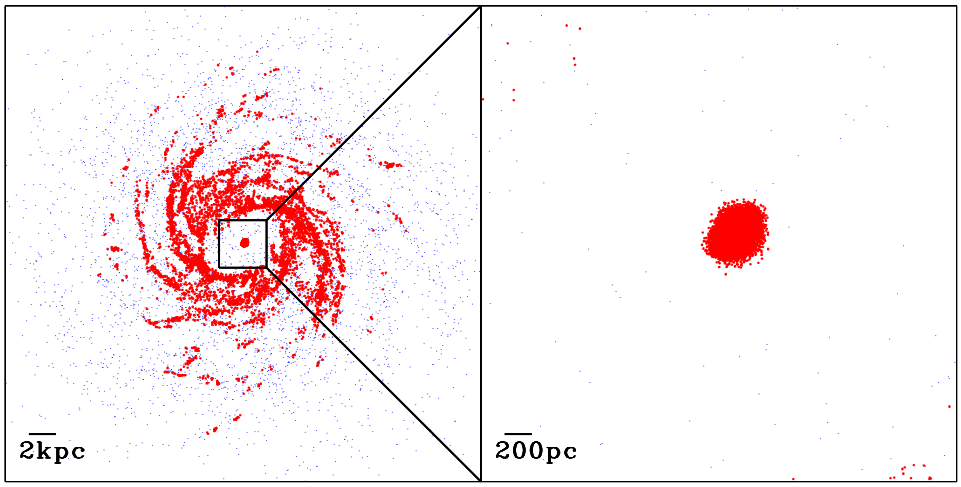

Figure 4. The distributions of gas with $f_{\rm H_2} < 0.01$ (blue) and $f_{\rm H_2} \geqslant 0.01$ (red) projected onto the x-y plane at $T = 2.3$ Gyr in the fiducial MW-type disk model M1.

('kinematic feedback'), respectively. The thermal energy is used for the 'adiabatic expansion phase', where each SN can remain adiabatic for a timescale of $t_{\rm adi}$. Although $t_{\rm adi} = 10^5$ yr is reasonable for a single SN explosion, we adopt a much longer $t_{\rm adi}$ of $\sim 10^6$ yr. This is mainly because multiple SN explosions can occur for a gas particle with a mass of $10^5 {\rm M}_\odot$ in these galaxy-scale simulations, and $t_{\rm adi}$ can be different for multiple SN explosions in a small local region owing to complicated interaction between gaseous ejecta from different SNe. Such interaction of multiple SN explosions would make the adiabatic phase significantly longer in real ISM of galaxies.

2.4 IMF

We adopt a canonical stellar initial mass function (IMF) proposed by Kroupa (2001), which has three different slopes at different mass ranges. Our recent study (Bekki 2013b, B13b) has shown that if the IMF depends on local physical properties of ISM (e.g., gas density and metallicity), then galaxy evolution, in particular, the time evolution of H_2 and dust contents, can be significantly influenced by the time-varying IMF. Since the main purpose of this study is not to demonstrate how the H_2 contents of disk galaxies can be influenced by a time-varying IMF, we assume that the IMF is fixed at the adopted Kroupa-IMF in the present study. It is our future works to clarify the roles of time-varying IMFs in controlling H_2 properties in galaxies with different masses and Hubble types.

2.5 Evolution of dust and metals

2.5.1 Chemical enrichment

Since the present model for chemical enrichment processes of galaxies is exactly the same as that used in B13a, we briefly describe the model here. Chemical enrichment through star formation and metal ejection from SNIa, II, and AGB stars is self-consistently included in the chemodynamical simulations. We investigate the time evolution of the 11 chemical elements of H, He, C, N, O, Fe, Mg, Ca, Si, S, and Ba in order to predict both chemical abundances and dust properties in the present study. We consider the time delay between the epoch of star formation and those of supernova explosions and commencement of AGB phases (i.e., non-instantaneous recycling of chemical elements).

We adopt the 'prompt SN Ia' model in which the delay time distribution (DTD) of SNe Ia is consistent with recent observational results by extensive SN Ia surveys (e.g., Mannucci et al. 2006). In this prompt SN Ia mode, there is a time delay ($t_{\rm Ia}$) between the star formation and the metal ejection for SNe Ia and the range of $t_{\rm Ia}$ is 0.1 Gyr $\leqslant t_{\rm Ia} \leqslant$ 10 Gyr. The fraction of the stars that eventually produce SNe Ia for 3–8$M_\odot$ has not been observationally determined. In the present study, $f_{\rm b} = 0.05$ is assumed. We adopt the nucleosynthesis yields of SNe II and Ia from Tsujimoto et al. (1995; T95) and AGB stars from van den Hoek & Groenewegen (1997; VG97) in order to estimate chemical yields in the present study.

2.5.2 Dust model

Since the dust model adopted in the present study is the same as those in B13a and B14, we here briefly describe the model. We calculate the total mass of jth component (j=C, O, Mg, Si, S, Ca, and Fe) of dust from kth type of stars (k = I, II, and AGB for SNe Ia, SNe II, and AGB stars, respectively) based on the methods described in B13a that is similar to those adopted in Dwek (1998, D98). We consider that the key parameter in dust accretion is the dust accretion timescale ($\tau_{\rm a}$). In the present study, this parameter can vary between different gas particles and is thus represented by $\tau_{{\rm a},i}$ for ith gas particle. The mass of jth component (j=C, O, Mg, Si, S, Ca, and Fe) of dust for ith gas particle at time t

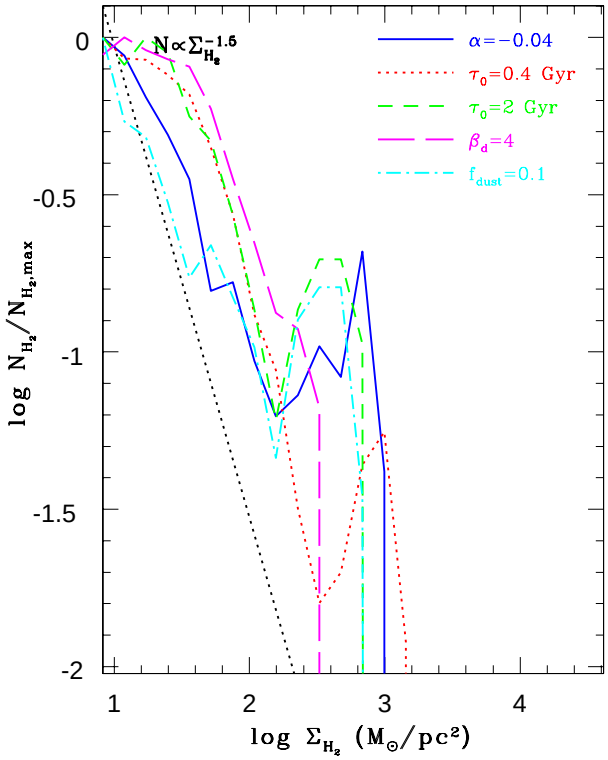

Figure 5. The H2SDD (H_2 surface density distribution) in different five MW-type disk models (M1): $\alpha = -0.04$ (blue solid), $\tau_0 = 0.4$ Gyr (red dotted), $\tau_0 = 2$ Gyr (green short-dashed), $\beta_{\rm d} = 4$ (magenta long-dashed), and $f_{\rm dust} = 0.1$ (cyan, dot-dashed).

$(d_{i,j}(t))$ can increase owing to dust accretion processes. The mass increase is described as

$$\Delta d^{\rm acc}_{i,j}(t) = \Delta t_i (1 - f_{{\rm dust},i,j}) d_{i,j}(t)/\tau_{{\rm a},i}, \quad (6)$$

where Δt_i is the individual time step width for the ith gas particle and $f_{{\rm dust},i,j}$ is the fraction of the jth chemical element that is locked up in the dust. Owing to this dust growth, the mass of jth chemical component that is *not* locked up in the dust $(z_{i,j}(t))$ can decrease, which is simply given as

$$\Delta z^{\rm acc}_{i,j}(t) = -\Delta t_i (1 - f_{{\rm dust},i,j}) d_{i,j}(t)/\tau_{{\rm a},i} \quad (7)$$

As is clear in these equations, the total mass of jth component in ith gas particle $(m_{i,j}(t))$ is $z_{i,j}(t) + d_{i,j}(t)$.

Dust grains can be destroyed though supernova blast waves in the ISM of galaxies (e.g., McKee 1989) and the destruction process is parameterized by the destruction time scale $(\tau_{\rm d})$ in previous one-zone models (e.g., Lisenfeld & Ferrara 1998; Hirashita 1999). Following the previous models, the decrease of the mass of jth component of dust for ith gas particle at time t due to dust destruction process is as follows

$$\Delta d^{\rm dest}_{i,j}(t) = -\Delta t_i d_{i,j}(t)/\tau_{{\rm d},i}, \quad (8)$$

where $\tau_{{\rm d},i}$ is the dust destruction timescale for ith particle. The dust destroyed by supernova explosions can be returned back to the ISM, and therefore the mass of jth chemical component that is not locked up in the dust increases as follows:

$$\Delta z^{\rm dest}_{i,j}(t) = \Delta t_i d_{i,j}(t)/\tau_{{\rm d},i} \quad (9)$$

Thus the equation for the time evolution of jth component of metals for ith gas particle are given as

$$z_{i,j}(t + \Delta t_i) = z_{i,j}(t) + \Delta z^{\rm ej}_{i,j}(t) + \Delta z^{\rm acc}_{i,j}(t) + \Delta z^{\rm dest}_{i,j}(t) \quad (10)$$

Likewise, the equation for dust evolution is given as

$$d_{i,j}(t + \Delta t_i) = d_{i,j}(t) + \Delta d^{\rm acc}_{i,j}(t) + \Delta d^{\rm dest}_{i,j}(t) \quad (11)$$

Dust is locked up in stars as metals are done so, when gas particles are converted into new stars.

2.5.3 Variable dust accretion models

We investigate the variable dust accretion ('VDA') model in which τ_a is different between different particles with different gaseous properties and changes with time according to the changes of gaseous properties. We need to introduce a few additional parameters in VDA in order to describe the possible dependences of $\tau_{\rm a}$ of gas particles on the gas densities, temperature, and chemical abundances. Our previous simulations with VDA (B14) clearly show the importance of dust accretion and destruction in the evolution of D and $f_{\rm H_2}$. The details of the VDA model is given in (B14), which discusses the comparison between the VDA and the constant dust accretion model in which $\tau_{\rm a}$ is constant for all particles throughout simulations.

We adopt the following dependence of $\tau_{{\rm a},i}$ on the mass density and temperature of a gas particle in the VDA:

$$\tau_{{\rm a},i} = \tau_0 (\frac{\rho_{{\rm g},0}}{\rho_{{\rm g},i}})(\frac{T_{{\rm g},0}}{T_{{\rm g},i}})^{0.5}, \quad (12)$$

where $\rho_{{\rm g},i}$ and $T_{{\rm g},i}$ are the gas density and temperature of

a i-th gas particle, respectively, $\rho_{\rm a,0}$ (typical ISM density at the solar neighborhood) and $T_{\rm g,0}$ (temperature of cold gas) are set to be 1 atom cm^{-3} and 20K, respectively, and τ_0 is a reference dust accretion timescale at $\rho_{\rm g,0}$ and $T_{\rm g,0}$. The dust destruction timescale, $\tau_{{\rm d},i}$, for each gas particle is described as follows:

$$\tau_{{\rm d},i} = \beta_{\rm d} \tau_{{\rm a},i}, \tag{13}$$

where β controls the timescale ratio of dust destruction to dust growth. In our previous studies (B13a, B14), $\beta_{\rm d} = 2$ is demonstrated to reproduce the observed dust properties of galaxies. We therefore consider that $\beta_{\rm d}$ should be adopted a reference value in the present dust model.

In the present study, the dust-to-metal-ratio of a galaxy is defined as follows:

$$f_{\rm dust} = \frac{M_{\rm dust}}{M_{\rm Z}}, \tag{14}$$

where $M_{\rm dust}$ and $M_{\rm Z}$ are the total amount of dust and metals in the galaxy, respectively. Although the initial value of $f_{\rm dust}$ could be different in different galaxies, we mainly adopt the standard value of 0.4 (corresponding to the value of the solar neighborhood) and thereby investigate the evolution of dust and H_2. We briefly discuss how the present results depend on the initial $f_{\rm dust}$ by changing $f_{\rm dust}$ from 0.1 to 0.4.

2.6 H_2 formation and dissociation

The model for H_2 formation and dissociation in the present study is exactly the same as those used in B13a: H_2 formation on dust grains and H_2 dissociation by FUV radiation are both self-consistently included in chemodynamical simulations. The temperature ($T_{\rm g}$), hydrogen density ($\rho_{\rm H}$), dust-to-gas ratio (D) of a gas particle and the strength of the FUV radiation field (χ) around the gas particle are calculated at each time step so that the fraction of molecular hydrogen ($f_{\rm H_2}$) for the gas particle can be derived based on the H_2 formation/destruction equilibrium conditions. Thus the H_2 fraction for i-th gas particle ($f_{{\rm H_2},i}$) is given as;

$$f_{{\rm H_2},i} = F(T_{{\rm g},i}, \rho_{{\rm H},i}, D_i, \chi_i), \tag{15}$$

where F means a function for $f_{{\rm H_2},i}$ determination.

Since the detail of the derivation methods of χ_i and $f_{{\rm H_2},i}$ (thus F) are given in B13a and B13b, we here briefly describe the methods. The SEDs of stellar particles around each i-th gas particles (thus ISRF) are first estimated from ages and metallicities of the stars by using stellar population synthesis codes for a given IMF (e.g., Bruzual & Charlot 2003). Then the strength of the FUV-part of the ISRF is estimated from the SEDs so that χ_i can be derived for the i-th gas particle. Based on χ_i, D_i, and $\rho_{{\rm H},i}$ of the gas particle, we can derive $f_{{\rm H_2},i}$ (See Fig. 1 in B13a). Thus each gas particle has $f_{{\rm H_2},i}$, metallicity ([Fe/H]), and gas density, all of which are used for estimating the IMF slopes for the particle (when it is converted into a new star).

The ages of stars ($t_{\rm s}$) are assumed to be 5 Gyr and 2 Gyr for the models with $z = 0$ and $z = 2$, respectively. The results of the present models are influenced by the choice of $t_{\rm s}$ only for the very early-phase of disk evolution ($T < 0.1$ Gyr), if $t_{\rm s}$ is rather short (~ 0.1 Gyr). The influences of $t_{\rm s}$ is very limited, because the photodissociation of H_2 by stars can be very efficient when gas is surrounded by very young stars and thus irradiated by the strong UV-radiation fields. We therefore discuss only the results of the models with $t_{\rm s}$ adopted above.

A number of previous theoretical models of H_2 formation (e.g., Hidaka & Sofue 2002) adopted the phase transition theory proposed by Elmegreen (1993), in which H I-to-H_2 transition in ISM is determined basically by gas pressure and radiation field. Elmegreen (1993) already showed that the observed H_2 mass function ($N \propto M^{-1.5}$) can be understood by his theory and also suggested that spiral density waves can convert H I into H_2. We do not adopt his phase transition theory but instead try to reproduce the observed H_2 properties using a different model based on H_2 formation on dust grains.

2.7 Gravitational dynamics and hydrodynamics

One of key ingredients of the code is that the gravitational softening length (ϵ) is chosen for each component in a galaxy (i.e., multiple gravitational softening lengths). Thus the gravitational softening length (ϵ) is different between dark matter ($\epsilon_{\rm dm}$) and gas ($\epsilon_{\rm g}$) and $\epsilon_{\rm dm}$ is determined by the initial mean separation of dark matter particles. The gravitational softening length for stars ($\epsilon_{\rm s}$) is set to be the same as that for gas. Initial $\epsilon_{\rm g}$ is set to be significantly smaller than $\epsilon_{\rm dm}$ owing to rather high number-density of gas particles. The softening length for new stars formed from gas is set to be the same as $\epsilon_{\rm g}$. Furthermore, when two different components interact gravitationally, the mean softening length for the two components is applied for the gravitational calculation. For example, $\epsilon = (\epsilon_{\rm dm} + \epsilon_{\rm g})/2$ is used for gravitational interaction between The values of $\epsilon_{\rm dm}$ and $\epsilon_{\rm g}$ ($= \epsilon_{\rm s}$) are 2.1 kpc and 0.2 kpc, respectively, for the fiducial MW-type disk model.

We consider that the ISM in galaxies can be modeled as an ideal gas with the ratio of specific heats (γ) being 5/3. The gaseous temperature ($T_{\rm g}$) is set to be 10^4 K initially in all models. The basic methods to implement SPH in the present study are essentially the same as those proposed by Hernquist & Katz (1989). We adopt the predictor-corrector algorithm (that is accurate to second order in time and space) in order to integrate the equations describing the time evolution of a system. Each particle is allocated an individual time step width (Δt) that is determined by physical properties of the particle. The maximum time step width ($\Delta t_{\rm max}$) is 0.01 in simulation units, which means that $\Delta t_{\rm max} = 1.41 \times 10^6$ yr in the present study. Although a gas particle is allowed to have a minimum time step width of 1.41×10^4 yr in the adopted individual time step scheme, no particle actually has such a short time step width ($\sim 10^4$ yr) owing to conversion from gas to star in high-density gas regions. The radiative cooling processes are properly included by using the cooling curve by Rosen & Bregman (1995) for $100 \leqslant T < 10^4$K and the MAPPING III code for $T \geqslant 10^4$K (Sutherland & Dopita 1993).

2.8 Tidal interaction model

In order to investigate how external tidal perturbation can influence the physical properties of H_2 in disk galaxies, we investigate tidal interaction models in which two disk galaxies strongly interact with each other. One of the two galaxies

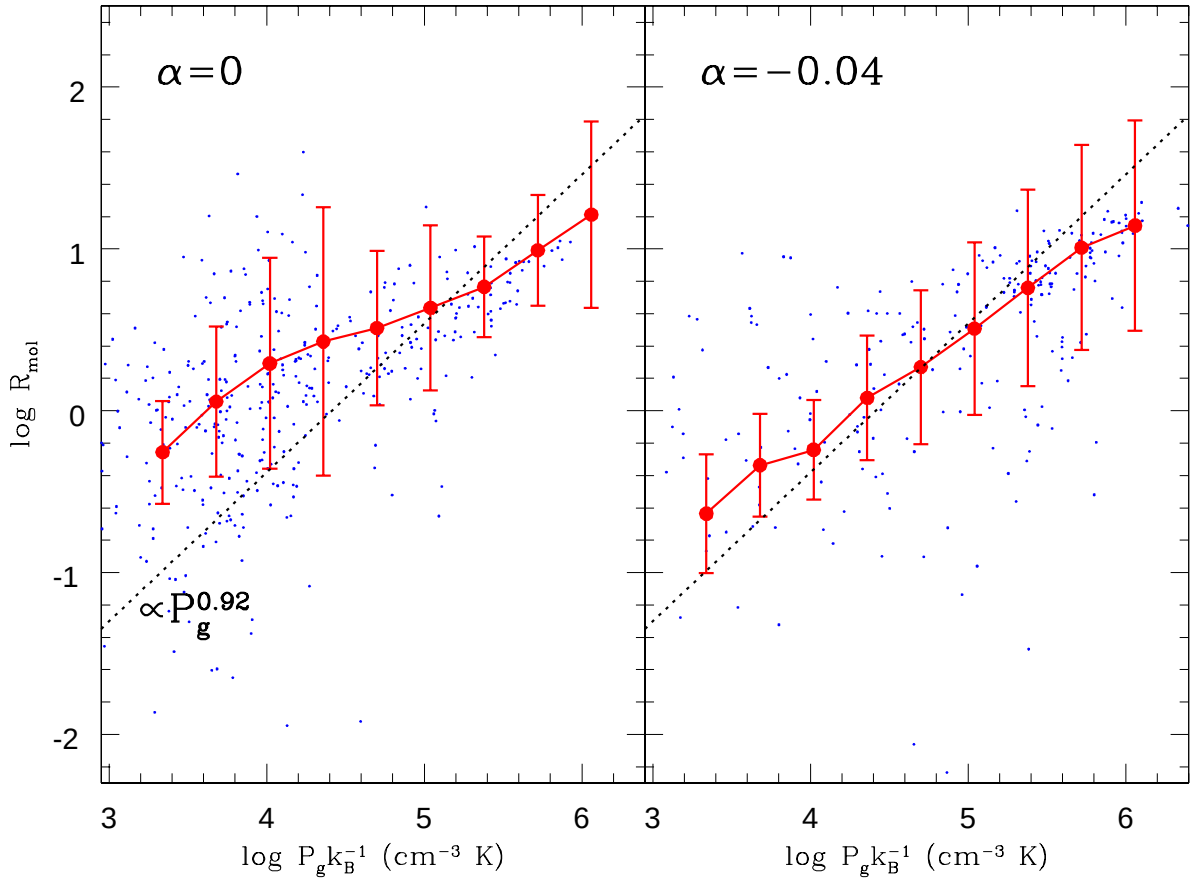

Figure 6. The plots of gas particles on the $R_{\rm mol} - P_{\rm g}$ plane in M1, where $R_{\rm mol}$ is the mass-ratio of H_2 to H I and $P_{\rm g}$ is gaseous pressure. Here $P_{\rm g}k_{\rm B}^{-1}$ rather than $P_{\rm g}$ is plotted for each gas particle so that the simulated correlation can be compared with the observed one (black dotted line) by Blitz et al. (2007). The red big circles indicate the mean $R_{\rm mol}$ for each $P_{\rm g}$ bin and the error bar shows the dispersion in $R_{\rm mol}$. The models with $\alpha = 0$ (flat metallicity gradient) and -0.04 (steeper one) are shown in the left and right panels, respectively.

('primary galaxy') is represented by the disk galaxy model described above whereas the interacting companion galaxy is represented by a point-mass particle. Although the mass-ratio of the companion to the primary can be a free parameter represented by m_2, we present the results only for the models with $m_2 = 1$ in which the influences of tidal interaction on H_2 properties can be clearly seen.

In all of the simulations of tidal interaction, the orbit of the two disks is set to be initially in the xy plane and the distance between the center of mass of the two disks is set to b $10R_{\rm d}$ (corresponding to 175 kpc for the MW-type disk model) for most models. The pericenter distance, represented by $r_{\rm p}$, is set to be $3R_{\rm s}$. The eccentricity is set to be 1.0 for all models of galaxy interaction, meaning that the encounter of galaxy interaction is parabolic. The spin of the primary galaxy in an interacting pair is specified by two angle θ and ϕ (in units of degrees), where θ is the angle between the z axis and the vector of the angular momentum of a disk and ϕ is the azimuthal angle measured from x axis to the projection of the angular momentum vector of a disk on to xy plane.

In the present study, we present the results of the following four tidal interaction models: (i) prograde ('PR') model with $\theta = 0$, $\phi = 0$, and $r_{\rm p} = 3R_{\rm s}$, (ii) retrograde ('RE') model with $\theta = 180$, $\phi = 0$, and $r_{\rm p} = 3R_{\rm s}$ (iii) highly inclined model with $\theta = 30$, $\phi = 60$, and $r_{\rm p} = 3R_{\rm s}$, and (iv) distant interaction model with $\theta = 0$, $\phi = 0$, and $r_{\rm p} = 4R_{\rm s}$.

2.9 A parameter study to solve key questions

We investigate numerous models to try to answer the following key questions related to the origin of H_2 in disk galaxies: (i) how can H_2 gas distribute within disks ?, (ii) what determines the molecular gas (H_2) fractions in disk galaxies ?, (iii) what are the roles of galactic bulges in controlling H_2 properties of disk galaxies ?, (iv) can dust evolution influence the evolution of H I and H_2 in galaxies ?, (v) does galaxy interaction enhance H_2 contents of galaxies ?, (vi) is there any threshold gas density (or threshold galaxy mass) beyond which H_2 formation is possible ?, and (vii) can high-z disk galaxies can contain larger fractions of H_2 within disks ? It should be noted here that these are selected, because the present numerical code allows us to investigate these: other questions such as the influences of AGN and dust size evolution on H_2 evolution can not be addressed in the present study.

In order to address these questions, we mainly describe the results of the selected 34 models in the present study.

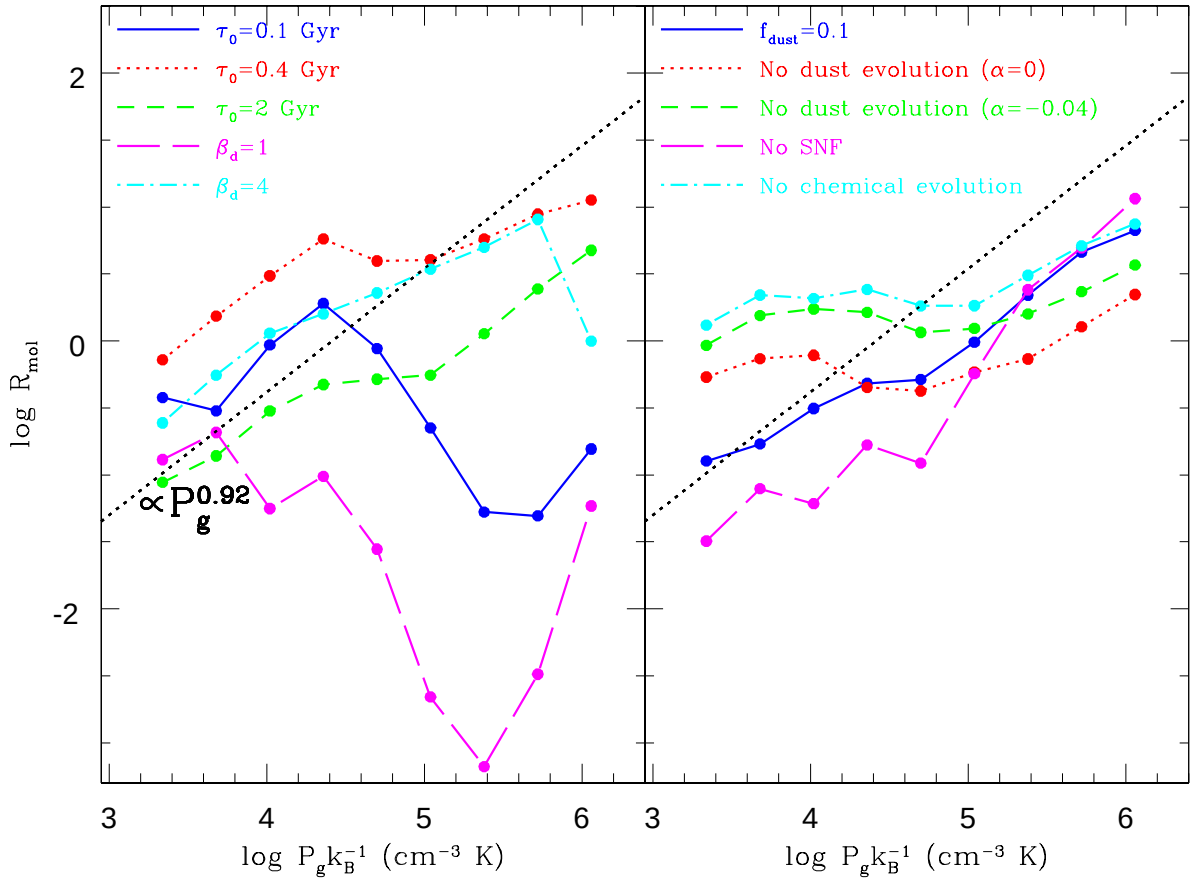

Figure 7. The same as as Fig. 5 but for different ten MW-type disk models (M1). The left panel shows the models with $\tau_0 = 0.1$ Gyr (blue solid), $\tau_0 = 0.4$ Gyr (red dotted), $\tau_0 = 2$ Gyr (green short-dashed), $\beta_{\rm d} = 1$ (magenta long-dashed), and $\beta_{\rm dust} = 4$ (cyan dot-dashed). The right panel shows the models with $f_{\rm dust} = 0.1$ Gyr (blue solid), no dust evolution and $\alpha = 0$ (red dotted), no dust evolution with $\alpha = -0.04$ (green short-dashed), no SN feedback effects (magenta long-dashed), and no chemical evolution (cyan dot-dashed).

We indeed investigated more than 34 models, in particular, for low-mass disk models in order to understand whether there can be a threshold halo mass beyond which H_2 formation is possible. However, we discuss only these results, because these representative models can more clearly show how the results depend on model parameters. The values of parameters adopted in these models are given in Table 2. In order to discuss the importance of dust evolution in H_2 evolution of galaxies, we investigate the models with different basic dust parameters. The parameter values for dust models and chemical evolution are summarized in Table 3. We first describe the results of the 'fiducial model' (M1) that corresponds to a disk galaxy similar to the Milky Way (thus referred to as MW-type disk model). Then we discuss how the key model parameters controls the H_2 properties of disk galaxies in detail.

2.10 A method to estimate H_2 surface density distribution (H2SDD)

The present chemodynamical models do not have enough spatial resolution to resolve the sub-pc-scale central cores of GMCs with H_2. We therefore can not discuss whether and where self-gravitating molecular clouds are formed in galactic gas disks. Instead of investigating the molecular cloud mass function (MCMF), we try to derive the H_2 surface density distribution (H2SDD), which would be useful in discussing the origin of MCMFs of galaxies. We estimate the H2SDD in a disk galaxy as follows. We first divide the simulated stellar disk region ($R_{\rm s} = 17.5$ kpc for the MW model) of a disk galaxy into 200×200 or 400×400 small meshes and thereby estimate the total mass of H_2 ($m_{\rm H_2,mesh}$).

We count the number of meshes ($N_{\rm H_2}$) with $m_{\rm H_2,mesh}$ within a given mass range so that we can estimate the H2SDD. The mesh size can be as small as $\sim$ 90pc for the MW-type disk models, which can be enough to discuss the mass of each individual H_2 gas clouds in a local region of a disk galaxy. Although this method is not exactly the same as that used in the observational estimation of MCMF, we consider that the derived H2SDD could be quite useful in discussing the origin of the observed MCMF in a qualitative manner (e.g., discussing the slope of the MCMF). We mainly check whether the simulated slope of H2SDD can be similar to the observed slope of the Galactic MCMF.

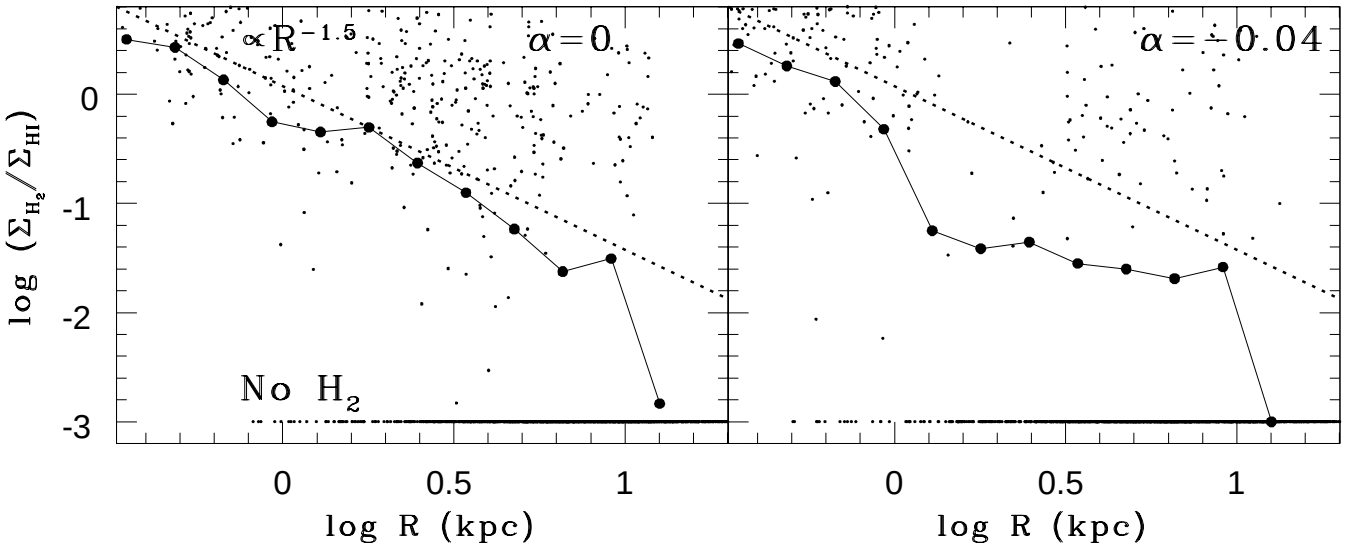

Figure 8. The projected radial distribution of the surface-density-ratios of H_2 to H I at $T = 1.1$ Gyr in the fiducial MW-type disk model (M1) with $\alpha = 0$ (left) and $\alpha = -0.04$ (right). The observed correlation ($\Sigma_{H_2}/\Sigma_{HI} \propto R^{-1.5}$) by Wong & Blitz (2002) is shown by a dotted line for comparison. The small dots represent the locations of the selected gas particles and the particles with no H_2 (i.e., $f_{H_2} = 0$) are shown at $\log(\Sigma_{H_2}/\Sigma_{HI}) = -3$ for convenience.

3 RESULTS

3.1 Fiducial MW model

3.1.1 Spatial distributions of hydrogen gas and H_2 *surface density distribution*

Figs. 1 and 2 describe how the spatial distributions of stars, H I, H_2, and dust evolve with time during the dynamical evolution of the gas disk with spiral arms and a central bar in the fiducial MW-type disk model (M1). Numerous spiral arms can be developed at $T = 0.6$ Gyr owing to gravitational instability, and they can influence the conversion from H I to H_2 in the gas disk after their formation. The locations of high-density H_2 regions at $T = 0.6$, 0.8, and 1.1 Gyr appear to be roughly coincident with the locations of H I spiral arms of the gas disk. However, H_2 shows a very clumpy distribution along spirals arms, which is in a striking contrast with the relatively smooth distribution of H I along spiral arms. This implies that only the high-density parts of the gaseous spiral arms can be the possible formation sites of H_2 in galactic disks. Numerous H_2 clumps can be active star-forming regions in the present SF model based on H_2 gas densities. Although the projected distribution of interstellar dust follows the spiral-like distribution of H I gas, it does not show clump-like structures as H_2. Interstellar dust can become less clumpy, because it can be efficiently destroyed by star-formation (i.e., SNe) which can occur in high-density gas clumps.

The physical roles of spiral arms in the formation of GMCs have been already discussed in a number of recent theoretical works based on high-resolution numerical simulations of gas disk evolution in disk galaxies (e.g., Dobbs et al. 2011; Wada et al. 2011; Halle & Combes 2013). Although these previous works did not self-consistently model the H_2 formation on dust grains and the time evolution of dust, they have already shown projected H_2 distributions in galactic disks (e.g., Fig. 14 in Halle & Combes 2013). The derived distributions of H_2 along spiral arms in the present MW-type disk model are similar to those reported in Halle & Combes (2013). The clumpy H_2 distributions derived in the present study are not so clearly seen in previous works, which could reflect the differences in the models of SF and SN feedback effects between the present and other works.

Fig. 3 shows the spatial distributions of H I and H_2 and the mass function of H_2 gas clouds (referred to as molecular cloud mass function; MCMF) in the gas disk at $T = 1.1$ Gyr in the fiducial MW-type disk galaxy model with $f_g = 0.09$. The simulated H_2 distribution is more centrally concentrated than H I gas within the disk owing to the more efficient formation of H_2 on dust grains in the inner part of the disk where both gas density and D can be higher during the disk evolution. The spatial distribution of H_2 gas shows small-scale clumpy structures within gaseous spiral arms where gas density can become rather large. Clearly, there is an outer truncation ($R \sim 13$ kpc) beyond which no/little H_2 gas can be found in this model. The projected radial density profile of H_2 is steeper than that of H I in this model.

The central part of the disk is dominated by H_2 gas and most of the gas particles there have rather high f_{H_2} (> 0.5), which implies that molecular hydrogen can be systematically more massive. The simulated H2SDD has a slope of ~ -1.5 for $\log \Sigma_{H_2} < 2.4$ $M_\odot$ pc^{-2}, which means that the simulated slope is similar to the observed slope of MCMF that is approximated as $N_{mc} \propto m_{mc}^{-1.5}$ for the MW and M31 (e.g., Fig. 4 in Fukui & Kawamura 2010). This implies that the present model of H_2 formation on dust grains is realistic and reasonable for H_2 formation in disk galaxies. Although the MCMF can be shifted toward higher masses if a coarser mesh size ($n_{mesh} = 200^2$) is used for the MCMF derivation, the slope of the MCMF does not change significantly.

This MW-type fiducial model can develop a central stel-

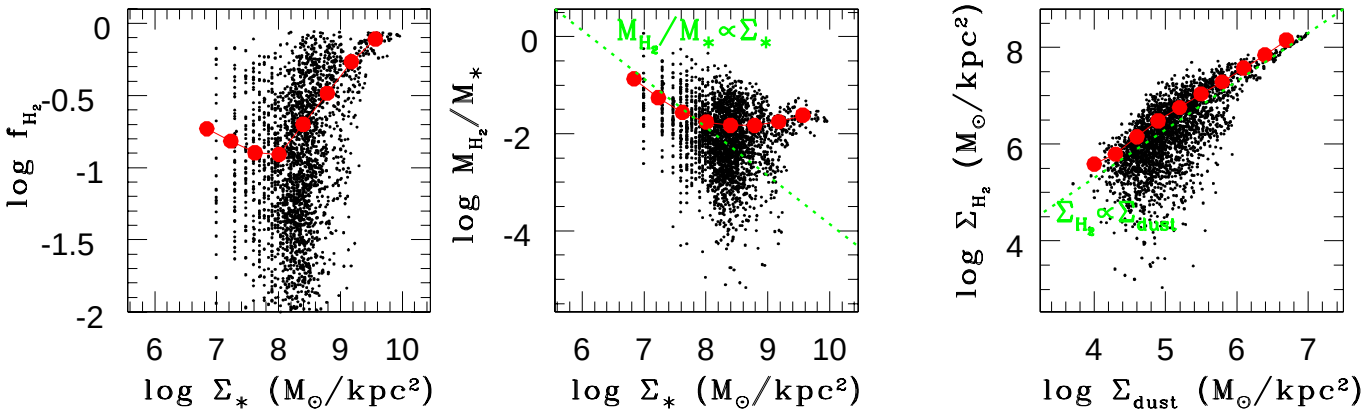

Figure 9. The simulated three H_2-scaling relations at $T = 1.1$ Gyr in the fiducial MW-type disk model (M1). The left, middle, and right panels show correlations between f_{H_2} and Σ_*, M_{H_2}/M_* and Σ_*, and Σ_{H_2} and Σ_{dust}, respectively. Small black dots indicate the physical properties (e.g., f_{H_2}) of local regions (represented by gas particles) whereas big red dots indicate the average values at each bin. For comparison, the linear correlations of $M_{H_2}/M_* \propto \Sigma_*$ and $\Sigma_{H_2} \propto \Sigma_{dust}$ are shown by green dotted lines in the middle and right panels, respectively.

lar bar owing to bar instability and the stellar bar can influence the formation process of H_2 significantly. The formation process of the stellar bar in the central 2 kpc and its influence on gas for $T \leqslant 1.1$ Gyr are given in Appendix A. Fig. 4 shows that the gas disk has a very strong concentration of H_2 in the central 200 pc at $T = 2.3$ Gyr. This H_2 concentration corresponds to the formation of nuclear H_2 gas disk due to the dynamical action of the central stellar bar on the surrounding gas. Owing to the rather high concentration of H_2 in the disk, the SFR can be significantly increased, in particular, in the central region of this barred disk galaxy. Furthermore, the H_2 fraction can be significantly increased (from $f_{H_2} \sim 0.1$ to ~ 0.3). Thus these results clearly demonstrate that stellar bars can play a vital role in converting H I to H_2 in disk galaxies.

Fig. 5 describes how the simulated H2SDDs depend on the model parameters for metallicity gradient and dust growth/destruction. The slopes of the H2SDDs do not depend strongly on the parameters, though some models (with steep metallicity gradient and longer dust accretion/destruction timescales) show the overproduction of high-density H_2 regions with $\log \Sigma_{H_2} > 2.4$ $M_\odot$ pc^{-2} within their disks. The larger number of high-density H_2 regions is due largely to the stronger central concentration of H_2 gas in the inner regions of the gas disks. As shown in Fig. 4, a central region of a galaxy is dominated by high-density H_2 gas so that almost all of the meshes in the central region can have high Σ_{H_2}. As a result of this, the simulated H2SDDs can have a bump around $\log \Sigma_{H_2} = 2.6 - 2.8$ $M_\odot$ pc^{-2}. It is a bit surprising that the simulated H2SDDs are less sensitive to the adopted dust model.

3.1.2 The fraction of molecular hydrogen

Fig. 6 describes the physical correlations between molecular fraction (R_{mol}), which is defined as the mass ratio of H_2 to H I, and $P_g k_B^{-1}$, where P_g is the gas pressure of a particle and k_B is the Boltzmann constant, in the gas disk of the fiducial MW model with different initial metallicity gradients $\alpha = 0$ and -0.04 dex kpc^{-1} at $T = 1$ Gyr. It should be stressed that this R_{mol} is not exactly the same as f_{H_2} ($= M_{H_2}/(M_{HI} + M_{H_2})$), which is often shown in figures of this paper. The observed correlation of $R_{mol} \propto P_g^{0.92}$ (e.g., Blitz et al. 2007; Fukui & Kawamura 2010) can be used as a key observational constraint for the present H_2 formation model. Although the dispersion in R_{mol} at each bin appears to be large, the two models show a clear positive correlation between R_{mol} and P_g (i.e., higher R_{mol} for higher gaseous pressure). This result implies that the present model for H_2 formation, which does not explicitly assume a dependence of H_2 formation efficiency on gaseous pressure, does a good job in predicting R_{mol} and its dependence on gaseous pressure.

Although the two models with different slopes of gaseous metallicity gradients ($\alpha = 0$ and -0.04) have the slopes of the $R_{mol} - P_g$ that are similar to the observed one ($R_{mol} \propto P_g^{-0.92}$), the model with a steep negative gradient of gaseous metallicity ($\alpha = -0.04$) can have the slope more similar to the observed one. The model with $\alpha = -0.04$ shows a lower H_2 formation efficiency at $P_g k_B^{-1} < 10^5$ (cm^{-3} K) in comparison with the model with $\alpha = 0$, mainly because the model with a negative metallicity gradient has a significantly lower dust-to-gas-ratio (i.e., lower metallicity) at the outer region of the disk with lower gaseous pressure so that H_2 formation efficiency on dust grains can become lower. The derived weaker dependence of the slope of the $R_{mol} - P_g$ relation on initial metallicity gradients implies that the slopes can be quite similar between different galaxies with different metallicity gradients.

Fig. 7 describes the simulated $R_{mol} - P_g$ relations in models with different model parameters for dust growth and destruction. These models have the parameter values being less realistic (e.g., rather long dust accretion timescale) in comparison with the models used in Fig. 6 so that we can discuss how the dust modeling is important for reproducing the observed $R_{mol} - P_g$ relation. It is clear from Fig. 7 that the simulated $R_{mol} - P_g$ relation in the model with shorter dust growth timescale ($\tau_0 = 0.1$ Gyr) is less consistent with the observed one owing to rather small R_{mol} at higher P_g ($> 10^5 k_B$) in the model. The model with a shorter dust destruction timescale ($\beta_d = 1$ and $\tau_0 = 0.2$ Gyr) can not

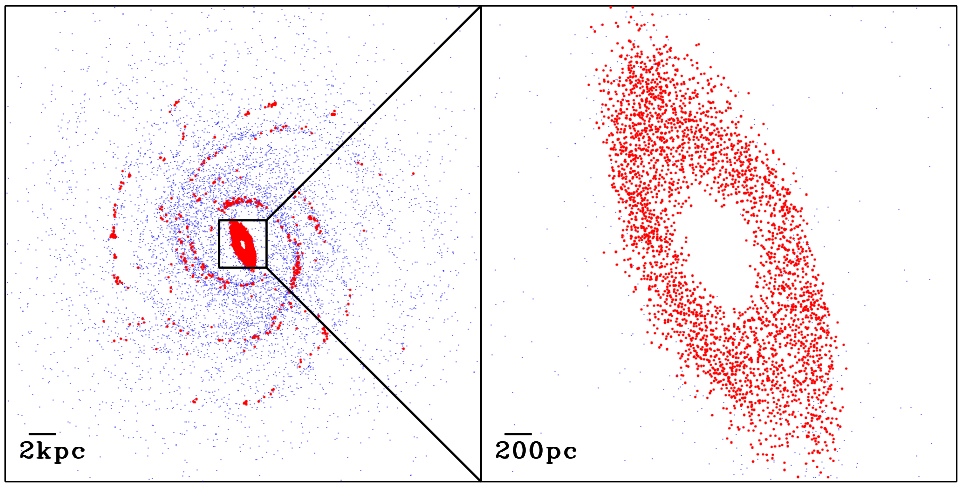

Figure 10. The distributions of gas with $f_{H_2} < 0.01$ (blue, H I) and $f_{H_2} \geqslant 0.01$ (red, H_2) projected onto the x-y plane at $T = 2.3$ Gyr in the big bulge model with $f_b = 1$ (M8). Clearly, an elongated H_2-ring can be seen in this model.

reproduce the observed $R_{mol} - P_g$ relation so well either. These results imply that both dust accretion and destruction timescales should be carefully chosen for reproducing the observed $R_{mol} - P_g$ relation.

The models with longer dust accretion timescale ($\tau_0 =$ 0.4 and 2 Gyr) show $R_{mol} - P_g$ similar to the observed one as long as $\beta_d = 2$ is adopted. However these models can not reproduce the observed $R_{mol} - P_g$ better than the models in Fig. 6, which implies that not only β_d but also τ_0 can be a key parameter for reproducing the observed $R_{mol} - P_g$. The slope of the simulated $R_{mol} - P_g$ in the model with a longer dust destruction time scale ($\beta_d = 4$ and $\tau_0 = 0.2$ Gyr) can better match the observed one except for rather high gaseous pressure ($P_g \sim 10^6 k_B$). The model with an initially lower dust-to-metal-ratio ($f_{dust} = 0.1$) shows $R_{mol} - P_g$ relation similar to those in Fig. 6, though R_{mol} at higher P_g is systematically smaller than those in Fig. 6 owing to the lower H_2 formation efficiency caused by the lower dust-to-gas ratio.

The models with no dust evolution show significantly shallower $R_{mol} - P_g$ relations, irrespective of the slopes of the initial radial metallicity gradients ($\alpha = 0$ and -0.04). This result implies that the time evolution of dust abundances in disk galaxies needs to be included for the self-consistent reproduction of the observed $R_{mol} - P_g$ relation. The models without SN feedback (SNF) and those without chemical evolution show significant deviation from the observed $R_{mol} - P_g$, which strongly suggests that dust growth and destruction processes caused by chemical enrichment and SN explosions need to be carefully included in reproducing the observed $R_{mol} - P_g$ relation in a quantitative manner. Thus these results demonstrate that as long as the H_2 formation processes on dust grains are included in hydrodynamical simulations of galaxy formation and evolution, the dust growth and destruction processes, which can be influenced by chemical enrichment and SN explosions, should be carefully considered in discussing the origin of the observed $R_{mol} - P_g$ relation.

3.1.3 Radial gradients of molecular fraction

The observed radial gradients of R_{mol} in disk galaxies (e.g., Wong & Blitz 2002) can be an additional constraint for any model for H_2 formation in galaxy-scale simulations. We here estimate R_{mol} at each radius in a simulated disk galaxy by calculating the ratio of Σ_{H_2} (i.e., the projected surface mass density of H_2) to Σ_{HI} at each radius in Fig. 8. Although individual gas particles corresponding to individual local gaseous regions in a disk galaxy have vastly different R_{mol} (ranging from 0 to 10), the slopes of the radial R_{mol} profiles in the two models with different α appear to be similar to the observed one ($R_{mol} \propto R^{-1.5}$). The model with $\alpha = 0$ can slightly better reproduce the observed slope than the model with $\alpha = -0.04$. Thus, the simulated slopes similar to the observed $R_{mol} \propto R^{-1.5}$ demonstrate that the present model for H_2 formation on dust grains is quite reasonable and realistic in discussing the global (galaxy-scale) distributions of neutral and molecular hydrogen in disk galaxies (as long as a reasonable set of model parameters for dust is adopted).

3.1.4 H_2 scaling relations

A number of recent observational studies have found intriguing correlations between physical properties of dust, gas, and stars in galaxies (e.g., Corbelli et al 2012; Cortese et al. 2012; Boselli et al. 2014). It is therefore essential for the present study to provide some comparisons between these observations and the corresponding simulation results. Fig. 9 shows that the H_2 fractions (f_{H_2}) are more likely to be larger for local regions with higher stellar surface densities (Σ_*), in particular, for $\Sigma_* > 10^8 M_\odot$ kpc^{-2}. There is a large dispersion in f_{H_2} for a given Σ_*, which reflects the fact that star formation histories and chemical enrichment processes

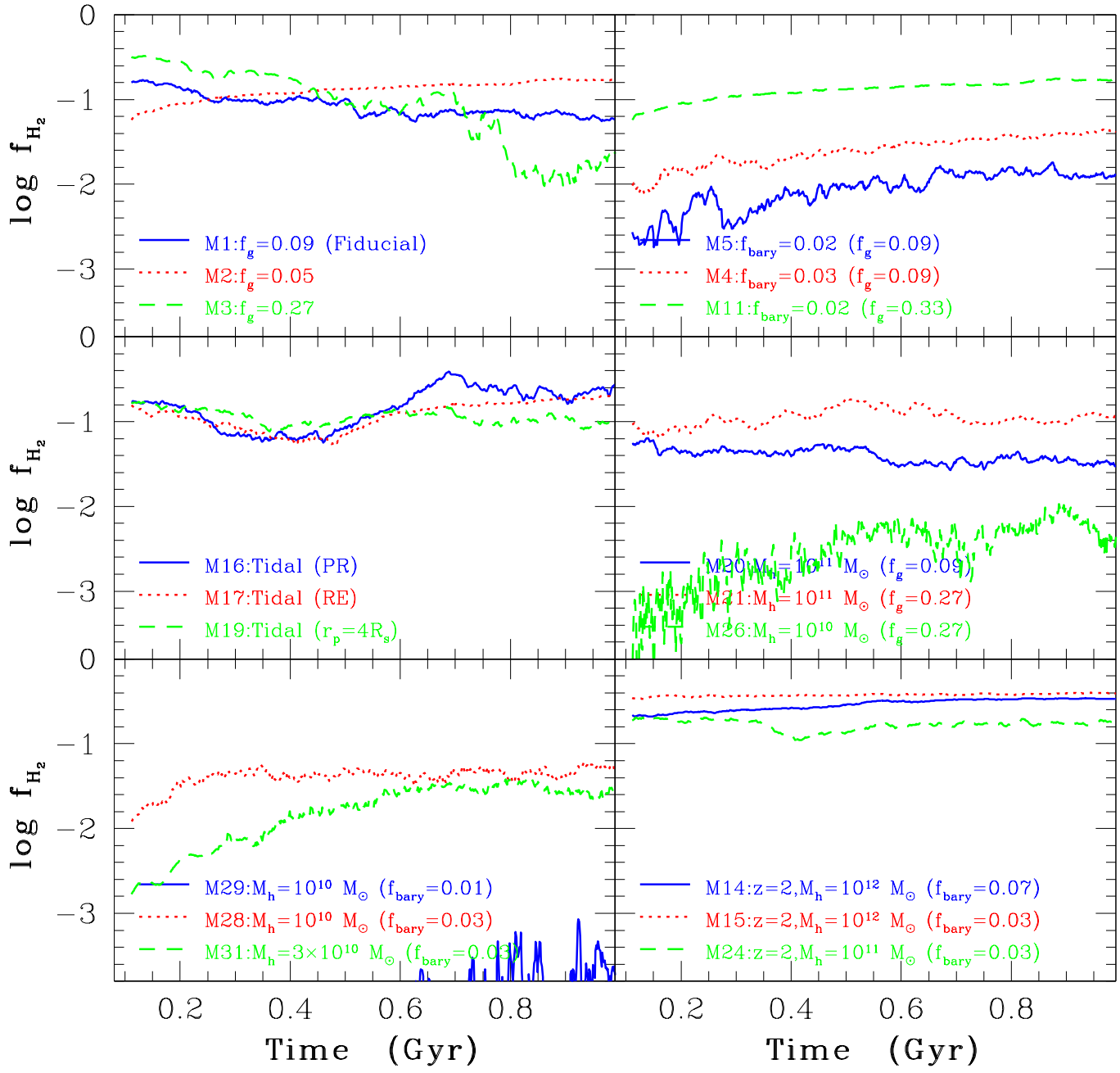

Figure 11. The time evolution of $f_{\rm H_2}$ in the representative 18 isolated and interaction models with different $f_{\rm g}$, $f_{\rm bary}$, $M_{\rm h}$, and z. Each panel includes only three models in which only one or two model parameters are different so that the roles of the parameter(s) in controlling the time evolution of $f_{\rm H_2}$ can be more clearly shown. For example, the top left panel describes how $f_{\rm g}$ can control $f_{\rm H_2}$ in disk galaxies.

(thus dust growth/destruction processes) are quite different in different local regions. The local regions with higher Σ_* can have higher gas densities so that conversion from H I to H_2 can occur more efficiently. This is a physical reason for the simulated trend of $f_{\rm H_2}$ with Σ_* in Fig. 9.

There is a positive correlation between the mass-ratio of H_2 to stars and Σ_*, though the correlation can not be simply described as a power-law profile owing to the flatter slope in the simulated relation at $\Sigma_* > 10^8 {\rm M}_\odot$ kpc^{-2}. A large dispersion in $M_{\rm H_2}/M_*$ can be seen, which again reflects the diverse histories of star formation and chemical enrichment in different local regions. The simulated relation between $\Sigma_{\rm H_2}$ and $\Sigma_{\rm dust}$ is relatively tight in comparison with other two correlations and can be described roughly as $\Sigma_{\rm H_2} \propto \Sigma_{\rm dust}$. These simulated relations between physical properties of dust, gas, and stars are at least qualitatively consistent with observational results (e.g., Boselli et al. 2014).

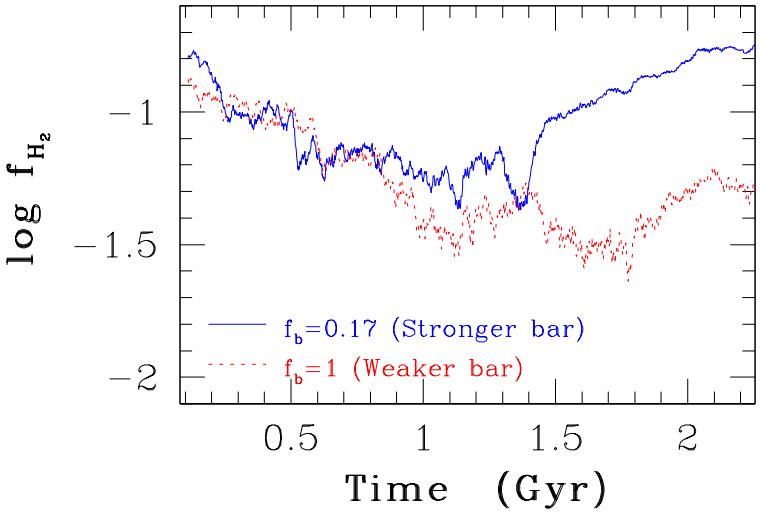

Figure 12. The long-term evolution of M_{H_2} (upper) and f_g (lower) in the two comparative models with $f_b = 0.167$ (M1, blue solid, smaller bulge) and $f_b = 1$ (M8, red dotted, bigger bulges). The disks with smaller bulges are more likely to develop stronger bars in their central regions owing to global bar instability in the present study. The stronger bars can dynamically act on gas disks so that a significant amount of gas can be transferred to the inner regions, where high-density H_2 regions can form. The later increase of f_{H_2} in the fiducial model with $f_b = 0.167$ is due to the central gas concentration in the disk caused by dynamical action of the bar (see also Fig. 4).

3.2 Parameter dependences

The physical properties of H_2 such as radial profiles of R_{mol} and time evolution of f_{H_2} can be quite diverse in the simulated disk galaxies with different model parameters. Since it is not so meaningful (and much less productive) to describe the results of all models in detail, we here describe only the results that are quite important and thus worth mentioning. In the following subsections, H_2 properties (e.g., f_{H_2}) are compared between models with different values of a model parameter (e.g., f_g) for a given set of other model parameters (i.e., other model parameters are fixed).

3.2.1 H_2 *morphology*

Although the morphologies of H_2 distributions in disk galaxies depend largely on the adopted f_b and f_g in disk galaxies, almost all models in the present study shows very strong central concentration of H_2 and clear coincidence between the locations of gas particles with high H_2 fractions and those of spiral arms in the disks. The distributions of H_2 along gaseous spiral arms appear to be very clumpy, which reflects the fact that only the high-density parts of the spiral arms can efficiently form H_2. These clumpy distributions are in a striking contrast with the H I distributions in disk galaxies.

Furthermore, the detailed spatial distributions of H_2 in the central few kpc of the disks can be controlled by the presence (or the absence) of stellar bars developed from bar instability in the central regions. Fig. 10 shows one of clear examples of the strong influences of the central stellar bars on the spatial distributions of H_2 in disk galaxies. Clearly, the disk galaxy in this model (M8) has a very elongated ring-like structure dominated by H_2, which is formed as a result of dynamical action of the central bar on the gas disk. This kind of 'molecular gas ring' can be seen in the models in which f_b is not so large and thus stellar bar formation can not be severely suppressed by the central big bulges.

3.2.2 Time evolution of f_{H_2}

The time evolution of f_{H_2} depend strongly on f_g, f_{bary}, f_b, M_h, and the formation redshifts of galaxies in the present models. Furthermore, tidal galaxy interaction can significantly change M_{H_2} and f_{H_2} depending on the orbit configurations of interacting two galaxies. The time evolution of 2D Σ_{HI} and Σ_{H_2} distributions for interacting galaxies is discussed in Appendix B, because the formation process of H_2 is quite interesting for interacting galaxies. The final 2D Σ_{HI} and Σ_{H_2} distributions for a high-z disk model are in a striking contrast with those of low-z disks and thus shown in Appendix B.

Since the time evolution of M_{H_2} and f_{H_2} are very similar in each model, we briefly summarize the derived key 7 dependences of f_{H_2} (not M_{H_2}) on the model parameters in Figs. 11 and 12. Firstly, f_{H_2} can be initially larger in the models with larger f_g for a given set of other model parameters (e.g., f_b). The final values of these two quantities ($T = 1$ Gyr) in the model with larger f_g (=0.27), however, can become rather small owing to rapid H_2 gas consumption by star formation. As a result of this, the model with larger f_g can have smaller final M_{H_2} and f_{H_2} than the model with smaller f_g (=0.09) . It should be noted that the final f_g in the model with $f_g = 0.27$ can become rather low too.

Secondly, f_{H_2} can be initially smaller in the models with smaller f_{bary} for a given f_g (and M_h), mainly because formation of non-axisymmetric structures such as bars and spirals can be suppressed in less strongly self-gravitating disks (owing to the dominant dark matter halos) so that H_2 formation efficiency can be lower. The lower surface gas densities in the models with smaller f_{bary} are also responsible for the

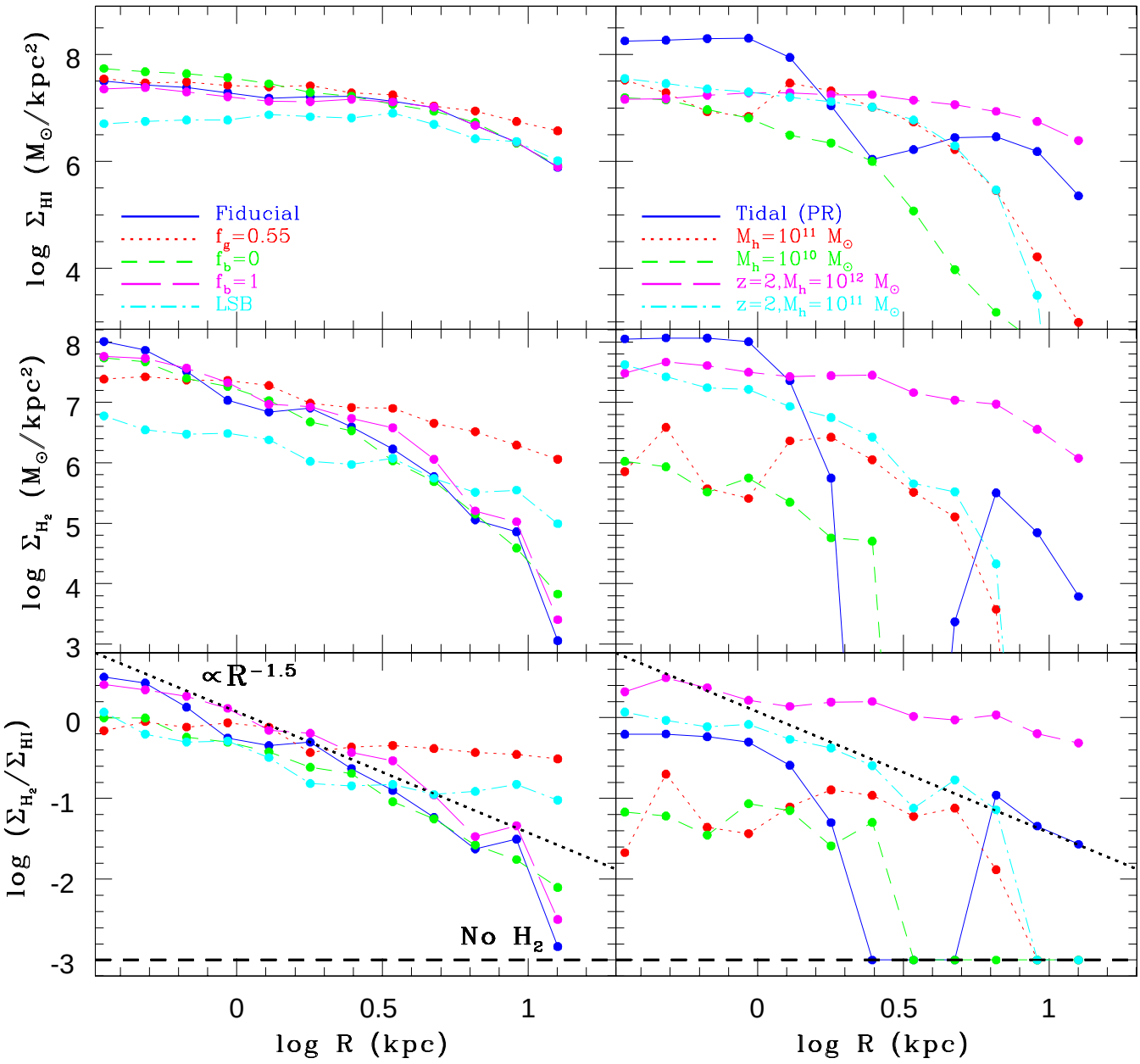

Figure 13. The projected radial density profiles of H I (top), H_2 (middle), and H_2-to-H I-ratio for different ten models. The left panel shows the MW-type disk models ($M_h = 10^{12}M_\odot$): M1 (blue solid, fiducial), M6 (red dotted), M7 (green short-dashed), M8 (purple long-dashed), and M13 (cyan dot-dashed, LSB). The right panel shows the five different models: M16 (blue solid), M21 (red dotted), M27 (green short-dashed), M15 (magenta long-dashed), and M24 (cyan dot-dashed).

smaller f_{H_2}. The smaller f_{H_2} for smaller f_{bary} can be seen in low-mass models with $M_h = 10^{10}M_\odot$. As shown in the model with smaller f_{bary} (0.02) yet larger f_g (=0.33), f_{H_2} can be larger than the model with $f_{bary} = 0.03$ and smaller f_g. Since gas consumption by star formation is slower in these models with smaller f_{bary}, the initial f_{H_2} difference in the models (i.e., larger f_{H_2} for larger f_g) can last for a long timescale.

Thirdly, f_{H_2} can be *initially* larger in the models with smaller bulges, because bigger galactic bulges can slow down or suppress the formation of spiral arms and bars so that H_2 formation efficiencies in gas disks can be also severely suppressed by the bulges. Fig. 12 shows that although f_{H_2} is initially larger in the model with $f_b = 0.17$ (fiducial model with a smaller bulge) than in the model with $f_b = 1$ ($T < 0.2$ Gyr), the f_{H_2} difference becomes smaller as the time passes by. After the formation of a stronger bar in the central region of the fiducial model, the bar dynamically acts on the gas disk so that a larger amount of gas can be transferred to the central region, where H_2 formation is enhanced. Consequently, f_{H_2} can become significantly larger at $T > 1.5$ Gyr. This kind of f_{H_2} enhancement by the dynamical action of a bar can occur to a lesser extend in the big bulge model with $f_b = 1$ in which only a weak stellar bar can be formed.

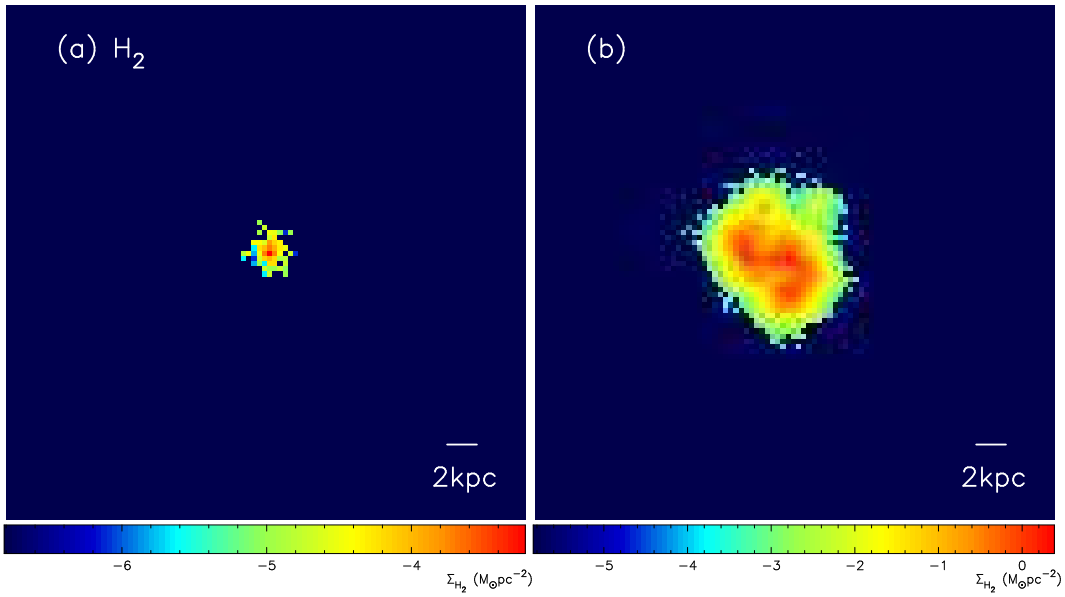

Figure 14. Th projected 2D H_2 density distributions (Σ_{H_2}) for the low-mass dwarf disk models ($M_h = 10^{10} M_\odot$), M25 with $f_g = 0.09$ ((a), left) and M26 with $f_g = 0.27$ ((b), right). Clearly, Σ_{H_2} is much lower in these low-mass models in comparison with the fiducial MW-type disk model.

It should be stressed here that the models (M9 and 12) with rather large f_b (2 and 4), initial f_{H_2} is rather low (< 0.05). However, the H_2 consumption by star formation is much less efficient in the models so that f_{H_2} can keep slowly rising (owing to the higher gas densities). As a result of this, these models can finally show larger f_{H_2} (> 0.1) at $T = 1.1$ Gyr. Therefore, we can not claim that disks with bigger bulges show smaller f_{H_2} in the present study. Fourthly, low surface brightness (LSB) disk galaxies can have initially smaller M_{H_2} and f_{H_2} owing to their low gas densities. It should be stressed that owing to much less rapid gas consumption and chemical enrichment, the LSB model can finally have M_{H_2} and f_{H_2} similar to those of the fiducial model.

Fifthly, galaxy interaction between two disk galaxies can significantly increase f_{H_2} after the pericenter passage. This enhancement of H_2 formation in disks can be more clearly seen in the 'prograde' tidal interaction model (PR) in which the spin axes of two disks are roughly parallel to those of their orbital angular momentum. This enhancement of H_2 formation, however, can not be clearly seen in other interaction models (RE or distant encounter models), which implies that not all of interacting galaxies show significantly large f_{H_2} in comparison with isolated field disk galaxies. Galaxy interaction can also change the distribution of H_2 and the MCMF, in particular, for the central region. The MCMFs of interaction models are discussed in Appendix A.

Sixthly, less massive disk galaxies can have smaller f_{H_2}, firstly because the formation of bars and spirals arms can be severely suppressed in the galaxies (owing to the stronger concentration of dark matter and smaller f_{bary}), and secondly because the dust-to-gas ratios (D), which are key factors for H_2 formation models of the present study, can be lower in the disks. The chemical enrichment processes by SNe and AGB stars in these low-mass models are so slow (owing to low SFRs) that D can not increase during the dynamical evolution of the disks. Therefore, the formation efficiencies of f_{H_2} can be kept lower in these models. The low-mass model with $M_h = 10^{10} M_\odot$ and smaller $f_{bary} = 0.01$ shows rather small f_{H_2}, which means that this low-mass disk galaxy is almost H_2-less. The baryonic fraction (f_{bary}) is particularly important in determining the time evolution of f_{H_2} for low-mass disk galaxies.

Seventhly, disk galaxies at higher z can have larger f_{H_2} than those at $z = 0$, mainly because disks are more compact so that a larger amount of H_2 gas can be formed in the high-density gaseous regions of the disks. It should be noted that (i) the simulated MW-type disk with low $f_g = 0.09$ at $z = 2$ can have a larger f_{H_2} (~ 0.32) and (ii) even the less massive disk with $M_h = 10^{11} M_\odot$ can have a larger f_{H_2} (~ 0.16). These results imply that high-z disk galaxies are highly likely to have systematically rather high H_2 gas fractions. The dependences of M_{H_2} and f_{H_2} on f_g and M_h can be seen among the simulated disk galaxies at $z = 2$.

3.2.3 Radial density profiles of H I and H_2

Fig. 13 shows that the five MW-type disk models with different f_g, f_{bary}, f_b, and surface stellar densities have qualitatively similar projected radial profiles of H I, H_2, and R_{mol}, though the absolute magnitudes of these surface mass densities are different between the models. The Σ_{H_2} profiles are steeper than Σ_{HI} in the five models, and the radial profiles of R_{mol} ($= \Sigma_{H_2}/\Sigma_{HI}$) have negative slopes (i.e., higher R_{mol} at smaller R). The MW-type disk models with different f_b have the steeper slopes approximated by $R^{-1.5}$ whereas the model with higher f_g (=0.55) and smaller $f_{bary} = 0.03$ and the LSB model have shallower R_{mol} profiles. The lower Σ_{H_2} in the model with larger f_g is due largely to rapid H_2 consumption in the inner disk.

Fig. 13 furthermore shows that tidal galaxy interaction can increase both Σ_{HI} and Σ_{H_2} significantly owing to the

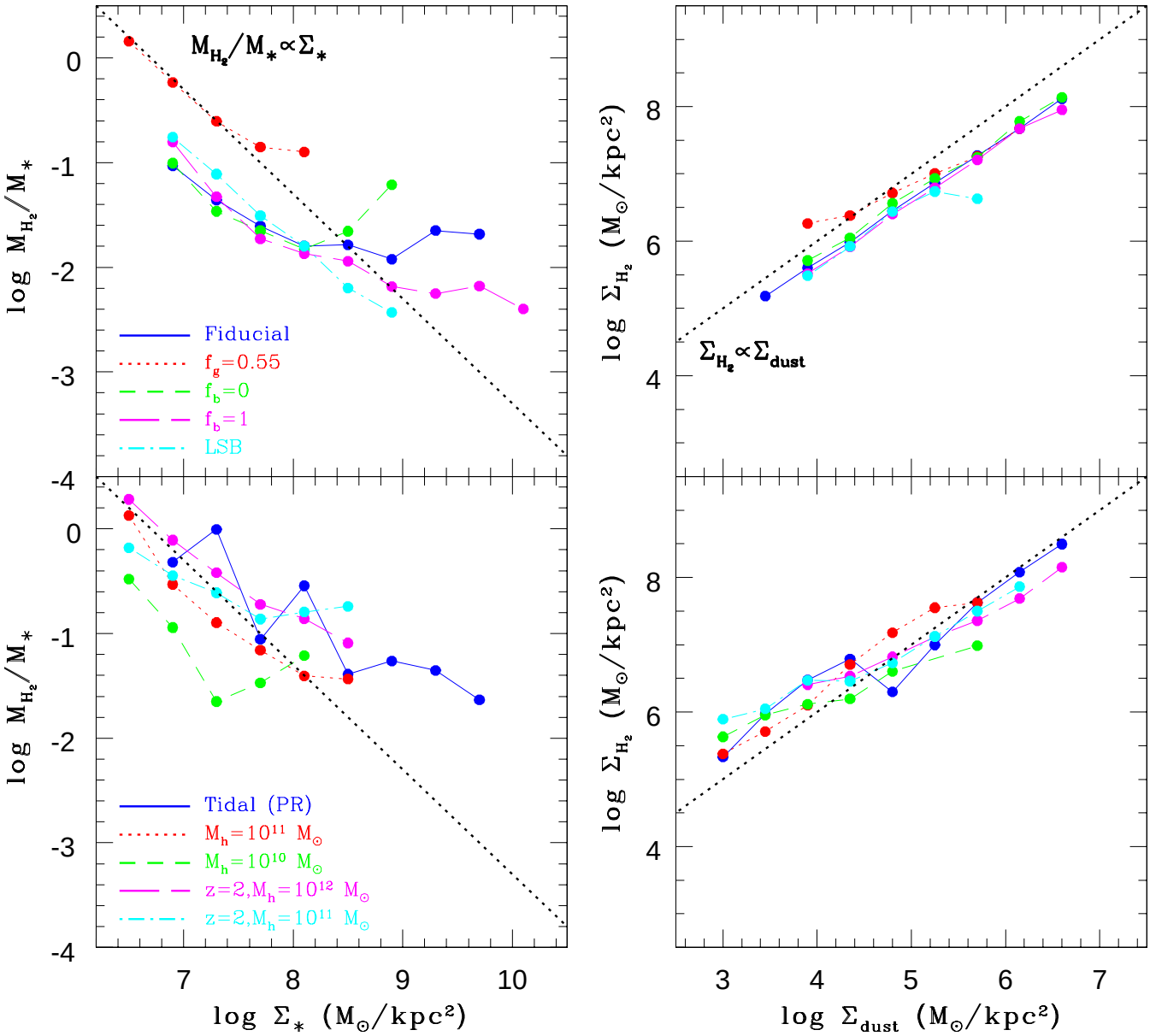

Figure 15. The simulated H_2-scaling relations for the representative ten models, which are the same as shown in Fig. 13. The left and right panels show correlations between M_{H_2}/M_* and Σ_* and Σ_{H_2} and Σ_{dust}, respectively. For comparison, the linear correlations of $M_{H_2}/M_* \propto \Sigma_*$ and $\Sigma_{H_2} \propto \Sigma_{dust}$ are shown by black dotted lines in the left and right panels, respectively.

strong gaseous concentration formed in the central regions of the interacting disks and the tidal arms. The strong central H_2 concentration is due largely to efficient gas-transfer to the nuclear region induced by tidal bar and gaseous dissipation. The formation of H_2 is more efficient in the central region and tidal arms during galaxy interaction, which is discussed in more detail in Appendix B. The radial profile of R_{mol} in the interaction model at $R < 1$ kpc is rather flat and there is the lack of H_2 gas in the circumnuclear region ($R \sim 2$ kpc) in the model.

The less massive disk models with $M_h = 10^{10} M_\odot$ and $10^{11} M_\odot$ have shallower Σ_{H_2} profiles thus shallower R_{mol} profiles too, which is in a striking contrast with the MW-type disk models. The origin of the low R_{mol} in low-mass disk models is closely associated with weak/no spiral and bar structures (due to the less strongly gravitation disks) and initially low D. Fig. 14 clearly demonstrates that if both f_g and f_{bary} are the same between the fiducial MW-type disk model and the low-mass dwarf disk model (M25 with $M_h = 10^{10} M_\odot$), then Σ_{H_2} is dramatically different between the two models. The maximum $\log \Sigma_{H_2}$ is only ~ -3.2 $M_\odot$ pc^{-2} in the low-mass disk model, which means that even if baryonic fractions are rather high, gas-poor low-mass disk galaxies are unlikely to form H_2 efficiently. A more gas-rich dwarf disk model shows a higher Σ_{H_2} along S-shaped gaseous region, but Σ_{H_2} is much lower than the MW-type disk model. The high-z disk models ($z = 2$) also have shallower R_{mol} profiles in the present study.

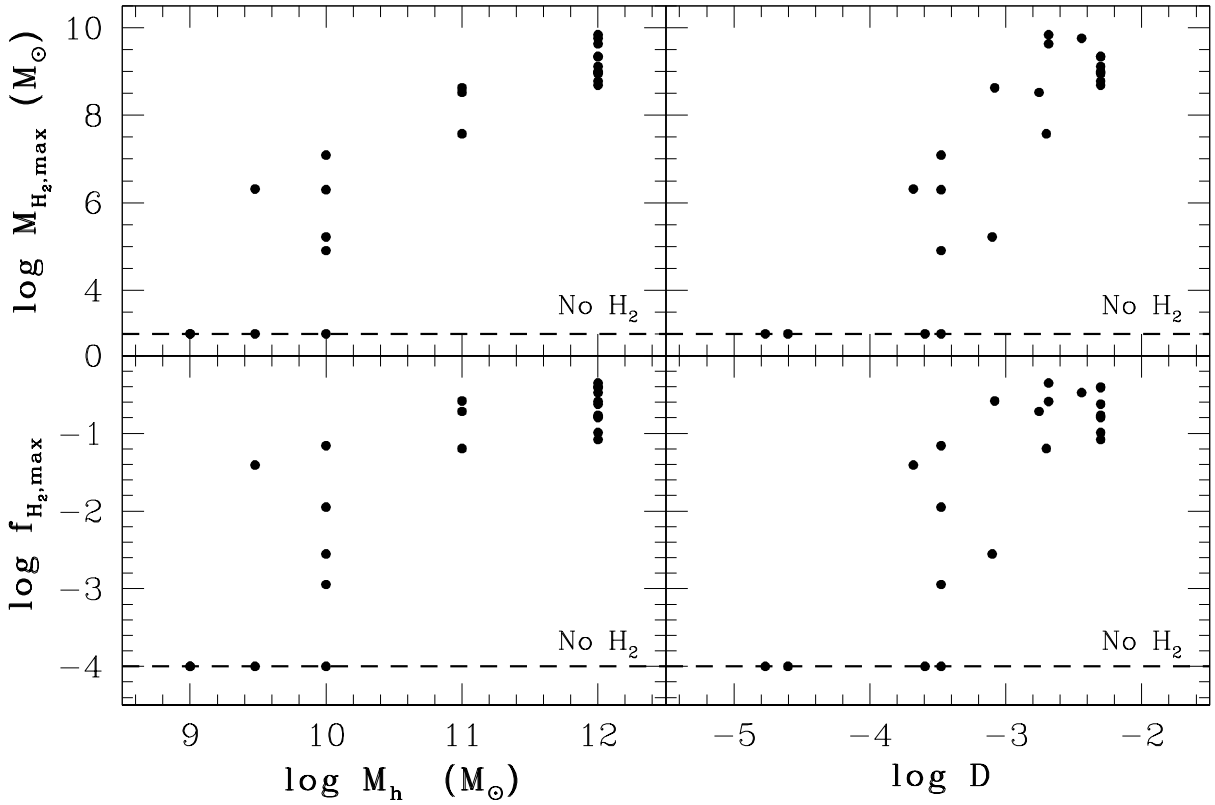

Figure 16. The dependences of the maximum M_{H_2} ($M_{H_2,max}$, upper) and f_{H_2} (f_{H_2}, lower) during 1.1 Gyr dynamical evolution of disks on M_h (left) and dust-to-gas-ratio D (right) in the selected 23 models. The models with no H_2 formation are plotted as $\log M_{H_2} = 3$ and $\log f_{H_2} = -4$ just for convenience. It should be noted that some low-mass dwarf models with $M_h \leqslant 10^{10} M_\odot$ have no H_2 (thus no SF), which means that these disks can be identified as 'H I dark galaxies'.

As shown in preceding sections, a strong central concentration of H_2 can occur in the barred disk galaxies owing to the dynamical action of stellar bars on gas. After the rapid consumption of H_2 gas in the centrally concentrated gas in the barred disk galaxies, there can be a deficiency of H_2 in their central regions. It is confirmed that the bulge-less disk galaxy with $f_b = 0$ at $T = 2$ Gyr (i.e., after long-term evolution), for which a strong bar can be spontaneously formed owing to global bar instability, can finally show the lack of H_2 in its central region after rapid H_2 consumption by star formation in the central region. This result implies that if gas accretion onto disks is truncated, even the late-type disk galaxies with no/little bulges can show the lack of H_2 gas in their central regions.

3.2.4 Internal H_2*-scaling relations*

Fig. 15 describes the physical correlations of local properties of H_2 with those of dust and stars within galaxies with different model parameters. These 'internal' H_2-scaling relations will be able to be compared with ongoing observational studies on H_2 properties of disk galaxies (by, e.g., ALMA), and thus the predicted scaling relations will be useful for interpreting the observational results. It is clear that the models with different f_g, f_b, and initial stellar mass densities of the disks have a similar positive correlation between M_{H_2}/M_* and Σ_* for $\log \Sigma_* < 8$ $M_\odot$ kpc^{-2}. The simulated relatively flat correlation for $\log \Sigma_* \geqslant 8$ $M_\odot$ kpc^{-2} is due to the strong concentration of H_2 in the central regions (where Σ_* is high) caused by dynamical action of the stellar bars on gas in the disks.

The tidal interaction model, in which f_{H_2} can be enhanced and H_2 distribution can be significantly changed, shows a $M_{H_2}/M_* - \Sigma_*$ relation similar to those seen in the isolated MW-type disk models, though the correlation is not so clear owing to the disturbed H_2 distribution. The less massive disk models with low M_h also show strong positive $M_{H_2}/M_* - \Sigma_*$ correlations for lower Σ_*, though the central H_2 concentration makes the correlation shallower for higher Σ_*. The high-z models with $z = 2$ also have clear positive $M_{H_2}/M_* - \Sigma_*$ correlations, which implies that a linear $M_{H_2}/M_* - \Sigma_*$ correlation will be identified in future observations of H_2 distributions in high$-z$ disk galaxies.

These ten models show a much tighter correlation between Σ_{H_2} and Σ_{dust}, which means that local ISM with higher dust surface densities can have higher H_2 surface densities in disk galaxies. This simulated almost linear $\Sigma_{H_2} - \Sigma_{dust}$ scaling relation is not so surprising, because H_2 formation efficiencies in local ISM are assumed to depend on the dust-to-gas ratios of local ISM in the present study. Recent observational studies have just started a detailed investigation on the sub-kpc-scale properties of dust in nearby disk galaxies like M31 (e.g., Viaene et al. 2014), which can be combined with the observed sub-kpc-scale properties of

H_2 to produce a possible dust-H_2 scaling relation within galaxies. The observed $\Sigma_{H_2} - \Sigma_{dust}$ scaling relation within galaxies will be able to be used as a stringent test for any theoretical model of H_2 formation on dust grains in galaxies.

3.2.5 Maximum possible H_2 *mass*

Fig. 16 describes the dependence of the maximum values of M_{H_2} and f_{H_2} during ~ 1 Gyr dynamical evolution on the initial halo masses (M_h) and dust-to-gas-ratios (D) in the selected models. It is clear from this figure that the models with larger M_h or larger D are more likely to have larger $M_{H_2,max}$ and $f_{H_2,max}$ The low-mass models have initially smaller D due to the adopted mass-metallicity relation, and spiral arms and bars, which are the major driver for efficient H_2 formation in disks, can not be formed owing to the less strongly self-gravitating disks (i.e., more strongly dominated by dark matter). This combination of the low D and the incapability of bar/spiral formation in the low-mass models is the main reason for the derived dependences of $M_{H_2,max}$ and $f_{H_2,max}$ on M_h and D.

It should be stressed here that some models with $M_h \leqslant 10^{10} M_\odot$ and those with $\log D < -4$ have no H_2 in the disks and thus no star formation in the present star formation models in which new stars can form exclusively from H_2 gas. This means that low-mass disk galaxies with very low D are dominated by H I gas and have no star formation so that they can be identified as isolated massive H I clouds with no star formation (in other words, 'dark H I galaxies'). The total H_2 mass can not become larger than $10^6 M_\odot$ in some of low-mass models with $M_h < 10^{10} M_\odot$, which means that massive star clusters and globular clusters are unlikely to be formed from GMCs in low-mass disk galaxies. We will discuss this point later in the Discussion section.

4 DISCUSSION

4.1 What determines f_{H_2} (R_{mol}) ?

One of the unresolved problems related to H_2 contents of galaxies dependent on Hubble types is that Sc/Sd late-type disks have smaller f_{H_2} (R_{mol}) in spite of their having larger gas masses with respect to their dynamical masses (M_{gas}/M_{dyn}, see Figs. 4 and 5 in YS91, as an example for this). Although this problem will be able to be better discussed in our forthcoming papers in which Λ CDM galaxy formation models with H_2 formation are adopted, we can discuss this problem based on the present new results. Galactic bulges have been demonstrated to suppress H_2 formation in ISM only for the early dynamical evolution of disk galaxies, if f_b is quite large ($1-4$, corresponding to Sa/S0 galaxies). The main reason for this is that spiral arms and bars, which can enhance the H_2 formation, can be suppressed by the presence of big bulges. The stronger ISRFs of big and dense bulges can be also responsible for less efficient conversion from H I to H_2 in ISM. Such a suppression effect of H_2 formation can be seen in models with different M_h and f_g.

However, the larger f_{H_2} in disks with smaller bulges can not last long owing to the more rapid gas consumption by star formation. Furthermore, big bulge can severely suppress the star formation so that f_{H_2} in disks with big bulges can steadily increase owing to chemical enrichment (i.e., increasing D) and finally become significantly larger. This means that although f_{H_2} can be larger in disks with smaller bulges *for a fixed* f_g, such disks do not necessarily continue to show larger f_{H_2} (particularly when there is no external gas supply). Also the initially larger f_{H_2} in disks with smaller bulges appears to be inconsistent with the observed trend of f_{H_2} with Hubble types. Given these results, it appears difficult to understand the origin of smaller f_{H_2} in late-type Sc/Sd galaxies in the context of the bulge effects on H_2 formation.

The central stellar bars formed from global bar instability have been demonstrated to enhance significantly f_{H_2} (R_{mol}), in particular, in the central regions of disk galaxies, though such enhancement can not last long owing to rapid gas consumption by star formation. Strong spirals arms have been demonstrated to be where H_2 formation is very efficient in the present study. Given that global bar/spiral instability can be prohibited by big bulges, disks with later types (i.e., smaller bulges) are more likely to have bars and thus show larger f_{H_2}. This possible trend of f_{H_2} with Hubble types is opposite to the observed trend, which implies that the formation efficiency of stellar bars is not the major factor that determines f_{H_2} in Sc/Sd galaxies.

The present study has also shown that the final f_{H_2} of disk galaxies depend on the initial baryonic mass fractions (f_{bary}) such that f_{H_2} can be larger in the models with larger f_{bary} for a given f_g (M_h). Recent observations have shown that f_{bary} can be smaller in galaxies with lower halo masses (e.g., Papastergis et al. 2012). These observations combined with the present results therefore imply that if the late-type Sc/Sd galaxies can be preferentially formed from dark halos with lower M_h, then the observed systematically small f_{H_2} can be more clearly explained. Although the observed luminosity functions for different Hubble types in the local field and the Virgo cluster suggests that Sa+Sb galaxies are systematically brighter than Sc+Sd galaxies (e.g., Binggeli et al. 1988), observational studies have not yet determined the mass functions of dark matter halos and baryonic fractions for different Hubble types. Therefore, it is unclear whether the above explanation for the observed small f_{H_2} in Sc/Sd galaxies is really plausible and realistic, though the smaller f_{bary} in later Hubble types would be a promising scenario.

4.2 Do dark H I galaxies exist ?

The present study has shown that low-mass disk galaxies show rather small $f_{H_2,max}$ (maximum possible H_2 fraction) and therefore can be identified as H I-dominated galaxies. The major physical reason for this very low H_2 contents is that these low-mass galaxies are extremely dust-poor so that they can not form H_2 on dust grains. The possible smaller f_{bary} in these low-mass galaxies can also contribute to the very low H_2 formation efficiency of the ISM. Furthermore, some of the simulated low-mass galaxies with rather high initial f_g (> 0.9) can show virtually $f_{H_2,max} = 0$, if M_h is as low as or lower than $3 \times 10^9 M_\odot$. These results imply that there would exist low-mass, and extremely low surface-brightness galaxies with only H I gas: These are almost 'dark' galaxies.

So far no observational studies have found strong evidence for the presence of *isolated* (or 'intergalactic') dark H I-rich galaxies with total gas masses larger than $10^6 M_\odot$ in the

nearby universe, though a number of observational studies investigated H I contents of galaxies in group environments (e.g., Kilborn et al 2005; Pisano et al. 2011). Although most of the detected H I objects have optical counterparts (or tidal origin) in these observations, a few observations so far discovered massive apparently isolated H I gas clouds with masses larger than $10^8 M_\odot$ (e.g., Davies et al. 2004; Kolibalski et al. 2004). These intriguing massive isolated objects are likely to be just tidal debris rather than dark H I galaxies (e.g., Bekki et al. 2005). If H I-dominated low-mass dark galaxies do not exist, the present study implies that such low-mass galaxies had lost almost all of their gas at their formation epochs or during their evolution owing to some physical processes such as ram pressure stripping and cosmic reionization.

4.3 Implications on the formation of globular clusters at high z

The present study has shown that (i) some low-mass galaxies with $M_{\rm h} \leqslant 10^{10} M_\odot$ can not form H_2 efficiently owing to their low dust masses and consequently (ii) the total H_2 masses are unlikely to exceed $10^7 M_\odot$. These results can have the following implications on the formation of massive star clusters, in particular, globular clusters (GCs), the origin of which remains unexplained. As recent theoretical studies of GC formation have demonstrated (e.g., D'Ercole et al. 2008; Bekki 2011), the initial stellar masses of GCs should be ~ 10 times larger than the present ones (typically, $2 \times 10^5 M_\odot$): Here we do not discuss the physical reasons for the proposed rather high initial masses of GC progenitor. This means that the original GMCs from which the initial massive stellar systems can form should be larger than $\sim 10^7 M_\odot$ even for a high star formation efficiency of ~ 0.2.

These theoretical results on GC formation combined with the present results imply that low-mass galaxies with $M_{\rm h} \leqslant 10^{10} M_\odot$ are unlikely to form GCs within them owing to the low H_2 contents. It would be possible that only low-mass, low-density star clusters, can form in their host low-mass galaxies. These low-mass clusters are prone to tidal destruction by their host galaxies so that they can finally become field stars within their hosts. If there exists a threshold halo mass above which GCs can form, then it can not only explain the observed absence of GCs in some faint dwarf galaxies in the Local Group (e.g., van den Bergh 2000) but also provide a physical basis on the minimum halo mass of GC host galaxies introduced in recent semi-analytic models of GC formation in galaxies based on hierarchical galaxy formation scenarios (e.g., Bekki et al. 2008; Griffen et al. 2010).

5 CONCLUSIONS

We have investigated the physical properties of H_2 in disk galaxies with different masses and Hubble types based on our new model for the formation of H_2 on dust grains. The basic parameters in this numerical study are $M_{\rm h}$ (halo mass), $f_{\rm bary}$ (baryonic mass fraction), $f_{\rm g}$ (gas mass fraction), and $f_{\rm b}$ (bulge-to-disk-ratio). We have investigated how the spatial distributions, time evolution, and scaling relations of H_2 depend on these parameters both for isolated disk galaxies and for interacting ones. The principal results are as follows.

(1) The observed positive correlation between the mass ratio of H_2 to H I ($R_{\rm mol}$) and gaseous pressure ($P_{\rm g}$) can be reproduced reasonably well by the present models. However, the $R_{\rm mol} - P_{\rm g}$ relation ($R_{\rm mol} \propto P_{\rm g}^{0.92}$) can be reproduced well only for some ranges of model parameters for dust growth and destruction. These results imply that dust can play a significant role in the formation of the $R_{\rm mol} - P_{\rm g}$ relation and thus that dust formation and evolution needs to be included in discussing the origin of H_2 scaling relations.

(2) The simulated H_2 surface density distributions (H2SDDs) in isolated luminous disk galaxies can have the slope of ~ -1.5 for $\log \Sigma_{\rm H_2} < 2.4$ $M_\odot$ pc^{-2}. The simulated slope is similar to the slope of the observed molecular cloud mass function for GMCs in the MW ($N_{\rm mc} \propto m_{\rm mc}^{-1.5}$). Although the simulated slopes of H2SDDs does not depend so strongly on galaxy parameters such as $f_{\rm b}$ and $f_{\rm gas}$ in isolated models, the mean $\Sigma_{\rm H_2}$ can be significantly increased in tidal interaction models.

(3) The simulated radial profiles of the $\Sigma_{\rm H_2}$-to- $\Sigma_{\rm HI}$-ratios in isolated luminous disk galaxies can be described as $R^{-1.5}$, which are observed in disk galaxies. This successful reproduction of observations implies that the present dust-regulated H_2 models can grasp some essential ingredients of H_2 formation in ISM of disk galaxies. The radial gradients can be different between low-mass and high-mass disk galaxies at low and high z and between isolated and interacting galaxies. The simulated H_2 distributions are clumpier than H I in most models. The H_2 surface density of a disk galaxy can dramatically drop beyond a certain radius where H_2 formation efficiency becomes rather low owing to the low gas density and the low D.

(4) The mass-ratios of H_2 to stars ($M_{\rm H_2}/M_*$) in individual local regions of a galaxy can anti-correlate with the local surface stellar density (Σ_*). This anti-correlation ($M_{\rm H_2}/M_* \propto \Sigma_*^{-1}$) can be seen in different galaxy models with different parameters. The H_2 surface densities ($\Sigma_{\rm H_2}$) of local individual regions in a galaxy can correlate with the dust surface densities ($\Sigma_{\rm dust}$) such that $\Sigma_{\rm H_2} \propto \Sigma_{\rm dust}$. This H_2-dust correlation is rather tight in different galaxy models.

(5) The initial total masses of dark halos ($M_{\rm h}$) can control the H_2 mass fractions ($f_{\rm H_2}$) of disk galaxies in such a way that $f_{\rm H_2}$ can be larger for larger $M_{\rm h}$. This is firstly because the formation of spiral arms and bars, where H_2 formation is rather efficient, can be severely suppressed in smaller $M_{\rm h}$, and secondly because the dust-to-gas-ratios (D), which determines the formation efficiency of H_2 on dust grains, are lower for smaller $M_{\rm h}$. Some low-mass galaxies with $M_{\rm h} \leqslant 10^{10} M_\odot$ show no/little H_2 formation within their disks in the present study.

(6) Galactic bulges can strongly suppress the formation of H_2 in gas disks at the early dynamical evolution of disk galaxies, if $f_{\rm b}$ is quite large ($\geqslant 1$). This is mainly because big bulges can prevent global spiral/bar instability from occurring so that efficient H_2 formation within spirals and

bars can be severely suppressed. This, however, does not necessarily mean that $f_{\rm H_2}$ can continue to be low, because slow gas consumption by star formation yet steady chemical enrichment (i.e., increasing D) can finally enhance $f_{\rm H_2}$ for some disk models with big bulges in the present study. These results imply that the origin of some late-type disk galaxies (Sc and Sd) with smaller $f_{\rm H_2}$ is not simply due to their small bulges. Some disk models in the present study show the lack of H_2 gas in their central regions.

(7) Barred disk galaxies are more likely to have larger $f_{\rm H_2}$ owing to the formation of centrally concentrated H_2 rings and disks. The central H_2 can be rapidly consumed by star formation so that higher $f_{\rm H_2}$ in barred galaxies can not last long without further external gas supply onto the disks. Some of the simulated barred disk galaxies can have elongated H_2-rings in their central regions, though such H_2 structures are short-lived. Bulge-less disk galaxies with central bars can also show the lack of H_2 in their central regions after rapid consumption of H_2 transferred to the inner few kpc.

(8) Disk galaxies at higher z are more likely to have larger $f_{\rm H_2}$ owing to their initially high gas densities in the more compact disks. This result does not depend on other model parameters such as $M_{\rm h}$. Disk galaxies with smaller $f_{\rm bary}$ at higher z can still show higher $f_{\rm H_2}$. For a given $M_{\rm h}$, $f_{\rm g}$, and z, disk galaxies with smaller $f_{\rm bary}$ have smaller $f_{\rm H_2}$. High-z disks are more likely to have very clumpy H_2 distributions with numerous small H_2 clouds.

(9) The maximum H_2 masses ($M_{\rm H_2,max}$) and fractions ($f_{\rm H_2,max}$) depend on initial halo masses $M_{\rm h}$ and dust-to-gas-ratios (D) such that both can be higher in larger $M_{\rm h}$ and larger D. For low-mass halos with $M_{\rm h} \leqslant 10^{10}{\rm M}_\odot$, the formation of H_2 can be completely suppressed in some models with smaller gas fractions so that no stars can be formed. Some low-mass galaxies with $M_{\rm h} \leqslant 3 \times 10^9{\rm M}_\odot$ can not form H_2 owing to rather low dust contents even if they are quite gas-rich $f_{\rm g} > 0.9$. These galaxies with no H_2 are still very rich in H I and could be observationally identified as gas-rich extremely low-surface brightness galaxies (or almost 'dark galaxies').

(10) The spatial distributions of H_2 in the simulated galaxies are quite diverse depending on initial $M_{\rm h}$ and Hubble types (e.g., bulge-to-disk-ratio, $f_{\rm b}$). Circumnuclear H_2 rings can be formed in barred disk galaxies, and such ring formation can significantly increase $f_{\rm H_2}$ in the galaxies. Radial H_2 profiles can be steeper for more luminous disk galaxies in isolation, and tidal interaction can dramatically increase the degrees of central H_2 concentration in disk galaxies.

(11) The present results have several important implications of star formation processes of galaxies. For example, massive star clusters, like old globular clusters, are unlikely to be formed in low-mass galaxies ($M_{\rm h} < 3 \times 10^9{\rm M}_\odot$), because the maximum possible total H_2 masses can be well less than $10^6{\rm M}_\odot$ (i.e., owing to the incapability of giant molecular clouds to form). This result implies that there would exist a threshold galaxy mass above which old GCs can be formed within galaxies at high z.

6 ACKNOWLEDGMENT

I (Kenji Bekki; KB) am grateful to the referee for constructive and useful comments that improved this paper. Numerical simulations reported here were carried out on the three GPU clusters, Pleiades, Fornax, and gSTAR kindly made available by International Center for radio astronomy research (ICRAR) at The University of Western Australia, iVEC, and the Center for Astrophysics and Supercomputing in the Swinburne University, respectively. This research was supported by resources awarded under the Astronomy Australia Ltd's ASTAC scheme on Swinburne with support from the Australian government. gSTAR is funded by Swinburne and the Australian Government's Education Investment Fund. KB acknowledges the financial support of the Australian Research Council throughout the course of this work.

REFERENCES

Andrievsky, S. M., Luck, R. E., Martin, P., Lépine, J. R. D. 2004, A&A, 413, 159
Bauermeister, A., et al. 2013, ApJ, 768, 132
Bekki, K., 2011, 412, 2241
Bekki, K., 2013, MNRAS, 432, 2298 (B13a)
Bekki, K., 2013, MNRAS, 436, 2254 (B13b)
Bekki, K., submitted to MNRAS (B14)
Bekki, K., Shioya, Y., 1998, ApJ, 497, 108
Bekki, K. Koribalski, B. S., & Kilborn, V. A., 2005, MNRAS, 363, L21
Bekki, K., Yahagi, H., Nagashima, M., Forbes, Duncan A., 2008, MNRAS, 387, 1131
Bigiel, F., Leroy, A., Walter, F., Brinks, E., de Blok, W. J. G., Madore, B., Thornley, M. D., 2008, AJ, 136, 2846
Binggeli, B., Sandage, A., Tammann, G. A., 1988, ARA&A, 26, 509
Blitz, L., Rosolowsky, E., 2006, ApJ, 650, 933
Blitz, L., Fukui, Y., Kawamura, A., Leroy, A., Mizuno, N., Rosolowsky, E., 2007, Protostars and Planets V, B. Reipurth, D. Jewitt, and K. Keil (eds.), University of Arizona Press, Tucson, 951 pp., p.81-96
Boselli, A., et al. 2014, A&A, 564, 67
Bruzual, G., Charlot, S., 2003, MNRAS, 344, 1000
Catinella, B., et al. 2010, MNRAS, 403, 683
Christensen, C., et al., 2012, MNRAS, 425, 3058
Combes, F., et al. 2014, A&A, 565, 97
Corbelli, E., 2012, A&A, 542, 32 (C12)
Cortese, L., et al. 2012, A&A, 540, 52
Davies, J., et al. 2004, MNRAS, 349, 922
D'Ercole, A., Vesperini, E., D'Antona, F., McMillan, S. L. W., & Recchi, S. 2008, MNRAS, 391, 825
Daddi, E., et al., 2010, ApJ, 713, 686
Dobbs, C. L., Burkert, A., Pringle, J. E., 2011, MNRAS, 417, 1318
Dwek, E., 1998, ApJ, 501, 643 (D98)
Elmegreen, B. G., 1993, ApJ, 412, 90
Fukui, Y., Kawamura, A., 2010, ARA&A, 48, 547

Galametz, M., Madden, S. C., Galliano, F., Hony, S., Bendo, G. J., Sauvage, M., 2011, A&A, 532, 56
Gould, R. J., Salpeter, E. E., 1963, ApJ, 138, 393
Griffen, B. F., Drinkwater, M. J., Thomas, P. A., Helly, J. C., Pimbblet, K. A., 2010, MNRAS, 405, 375
Halle, A. Combes, F., 2013, A&A, 559, 55
Herbst, E., 2001, Chem, Soc, Rev, 30, 168
Hernquist, L., & Katz, N., 1989, 70, 419
Hidaka, M., Sofue, Y., 2002, PASJ, 54, 223
Hirashita, H., 1999, ApJ, 522, 220
Hollenbach, D., Salpeter, E. E., 1971, ApJ, 163, 155
Lagos, C. P., Lacey, C. G., Baugh, C. M., 2012, in prepring (arXiv1210.4974)
Kennicutt, R. C., Jr., 1998, ApJ, 498, 541
Kilborn, V. A., Koribalski, B. S., Forbes, D. A., Barnes, D. G., Musgrave, R. C., 2005, MNRAS, 356, 77
Kroupa, P., 2001, MNRAS, 322, 231
Koribalski, B. S., et al. 2004, AJ, 128, 16
Krumholz, M. R., McKee, C. F., Tumlinson, J., 2009, ApJ, 693, 216
Leon, S., Combes, F., Menon, T. K., 1998, A&A, 330, 37
Leroy, A. K., et. al., 2011, ApJ, 737, 12
Lisenfeld, U., Ferrara, A., 1998, ApJ, 498, 145
Mckee, C. F., 1989, in IAU Symp. 135, Interstellar Dust, Edited by Louis J. Allamandola and A. G. G. M. Tielens, p43
Mannucci, F., Della Valle, M., Panagia, N., 2006, MNRAS, 370, 773
Mannucci, F., Della Valle, M., Panagia, N., 2006, MNRAS, 370, 773
Maoz, D., Sharon, K., Gal-Yam, A., 2010, ApJ, 722, 1879
Mori, M., Yoshii, Y., Nomoto, K., 1999, ApJ, 511, 585
Muñoz-Cuartas, J. C.; Macció, A. V., Gottlöber, S., Dutton, A. A., 2011, MNRAS, 411, 584
Navarro, J. F., Frenk, C. S., White, S. D. M., 1996, ApJ, 462, 563 (NFW)
Neto, A. F., 2007, MNRAS, 381, 1450
Papastergis, E., Cattaneo, A., Huang, S., Giovanelli, R., Haynes, M. P., 2012, ApJ, 759, 138
Pelupessy, F. I., Papadopoulos, P. P., van der Werf, P., 2006, ApJ, 645, 1024 (P06)
Pisano, D. J., Barnes, D. G., Staveley-Smith, L., Gibson, B. K., Kilborn, V. A., Freeman, Ken C., 2011, ApJS, 197, 28
Rosen, A., Bregman, J. N., 1995, ApJ, 440, 634
Saintonge, A., et al., 2011, MNRAS, 415, 61
Schmidt, M., 1959, ApJ, 129, 243
Schneider, R., Omukai, K., 2010, MNRAS, 402, 429
Scoville, N., et al. 2014, ApJ, 783, 84
Shull, J. M., 1978, ApJ, 226, 858
Stinson, G., Seth, A., Katz, N., Wadsley, J., Governato, F., Quinn, T., 2006, MNRAS, 373, 1074
Sutherland, R. S., Dopita, M. A., 1993, ApJS, 88, 253
Tacconi, L. J., et al., 2010, Nat, 463, 781
Theis, C., Orlova, N., 2004, A&A, 418, 959
Thornton, K., Gaudlitz, M., Janka, H.-Th., Steinmetz, M., 1998, ApJ, 500, 95
Tsujimoto, T., Nomoto, K., Yoshii, Y., Hashimoto, M., Yanagida, S., Thielemann, F.-K., 1995, MNRAS, 277, 945 (T95)
van den Hoek, L. B.; Groenewegen, M. A. T., 1997, A&AS, 123, 305 (VG97)
van den Bergh, S., 2000, The galaxies of the Local Group
Viaene, S., et al. 2014, accepted in A&A, (rrXiv:1403.4272)
Wada, K., Baba, J., Saitoh, T. R., 2011, ApJ, 735, 1
Wilson, C. D., et al., 2009, ApJ, 693, 1736
Wong, T., Blitz, L., 2002, ApH, 569, 157
Young, J. S., Scoville, N. Z., 1991, ARA&A, 29, 581
Yozin, C., Bekki, K., 2014a, accepted in MNRAS (arXiv1406.1642)
Yozin, C., Bekki, K., 2014b, MNRAS, 439, 1948
Zaritsky, D., Kennicutt, R. C., Jr., Huchra, J. P., 1994, ApJ, 420, 87

APPENDIX A: THE FORMATION OF A CENTRAL STELLAR BAR

In the present fiducial MW-type disk model (M1), a stellar bar can play a significant role in the formation of H_2 on dust grains and the dynamical evolution of H_2 gas, in particular, in the later evolution of the central region of the gas disk. We here briefly describe the bar formation process in this model. As shown in Fig. A1 on the time evolution of stellar surface density (Σ_s) of the disk, a stellar bar can start to develop around $T = 0.8$ Gyr owing to bar instability in this model with a relatively small bulge mass. The formation of a strong nuclear bar can be completed by $T = 1.1$ Gyr so that the bar can influence the gas dynamics there after its formation (e.g., a massive nuclear H_2 disk can be formed at $T = 2$ Gyr as a result of dynamical interaction between the bar and H_2 gas, as shown in Fig. 4). The gaseous component (H I+H_2) also shows a bar-like distribution in the central region of the disk when the stellar bar forms at $T = 1.1$ Gyr.

APPENDIX B: INTRIGUING H_2 DISTRIBUTIONS IN SELECTED MODELS

Figs. B1 and B2 show intriguing H_2 distributions of galactic disks in selected models. In Fig. B1, the initial Σ_{H_2} of each mesh at $T = 0$ is calculated by assuming that H_2 mass fraction is 0.01 just for convenience, because H_2 formation efficiency based ISRF etc is not calculated at $T = 0$. The formation efficiency of H_2 on dust grains can be significantly enhanced in the strong tidal arms of the interacting disk galaxy for the prograde interaction model (M16), as shown in Fig. B1 (at $T = 0.6$ Gyr). During the efficient gas infall onto the nuclear regions, both H I and H_2 gas densities can become significantly higher so that star formation rates can be high in the nuclear region and the tidal arms. After tidal interaction, the H_2 distribution appears to be clumpy with a number of off-center high-density H_2 clumps in the disk. Such off-center massive gas clumps can be also seen in recent models of gas-rich interacting galaxies by Yozin & Bekki (2014b). Since the number of tidal interaction models investigated in the present study is rather small (< 10), we can not conclude whether such a clumpy H_2 distribution is a characteristic of post-interacting galaxies. We will investigate this point in our future works by performing a larger number of numerical simulations of interacting galaxies with a much wider range of model parameters for galaxy interaction.

Fig. B2 shows that a gas-rich, more compact disk at

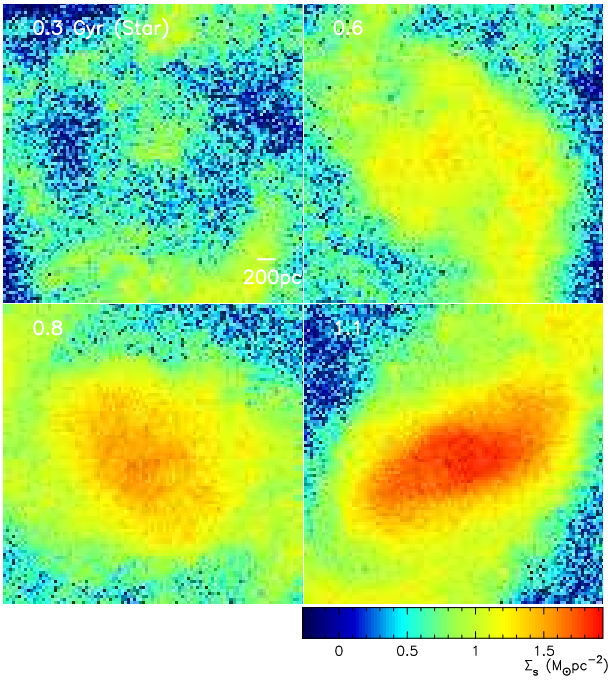

Figure A1. The time evolution of the projected mass densities for stars (Σ_s) in the central region of the fiducial MW-type disk model (M1). The formation of a central stellar bar can be developed within less than 1 Gyr in this model so that the bar can influence the formation of H_2 there.

$z = 2$ can have a widespread spatial distribution of H_2 gas in the model M15. In this model, the baryonic mass fraction is lower than the fiducial MW-disk model (i.e., less strongly self-gravitating) so that the formation of a strong bar can be suppressed. Therefore, a bar-like distribution of gas can not be clearly seen in this model. Even in the outer part of the gas disk, high-density H_2 regions can be seen, which is in a striking contrast with the H_2 distribution of the low-z fiducial MW-disk model (M1). The gas disk at $z = 2$ appears to be composed of numerous small H_2 clumps, which implies that the mass function of molecular clouds (MCMF) can be significantly different between $z = 0$ and $z = 2$. Since the present simulation does not have enough resolution to investigate MCMFs, we will discuss this point in our future numerical works with a much larger number of gas particles.

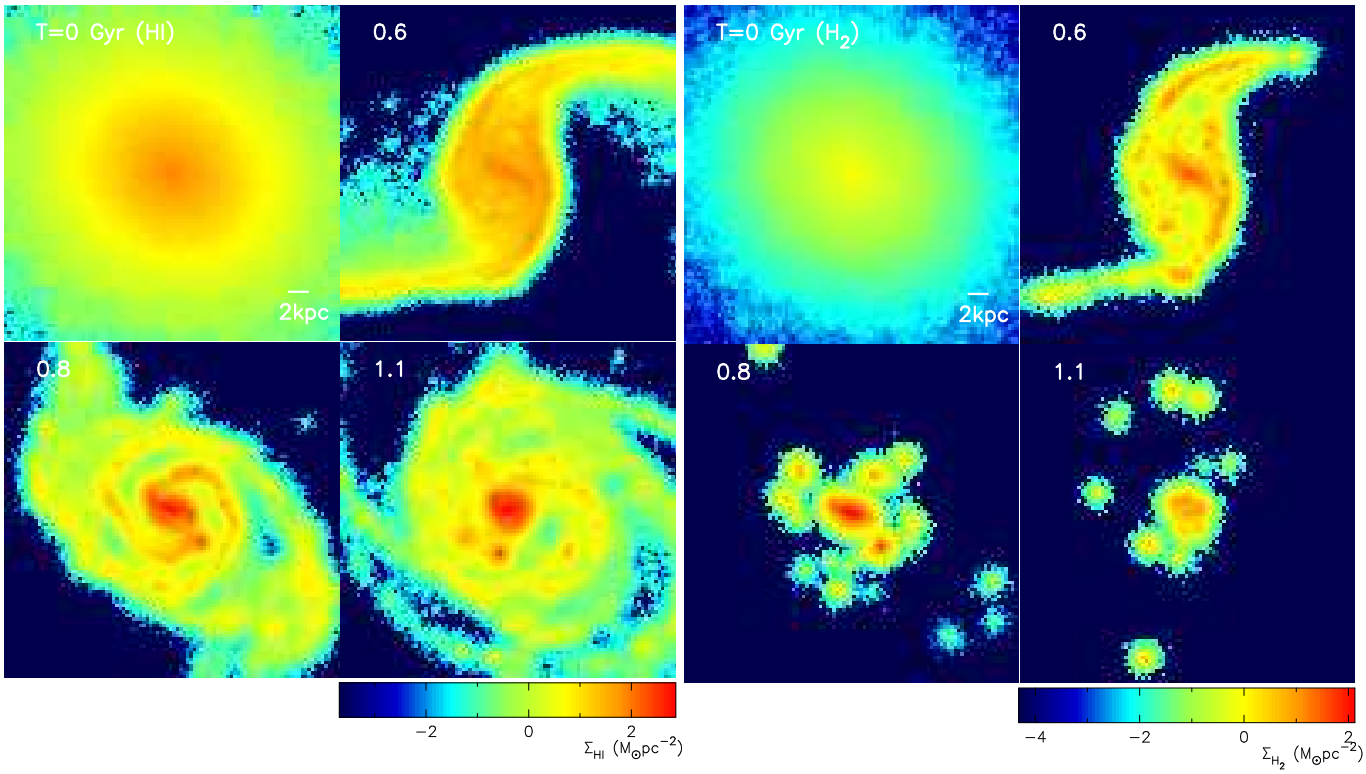

Figure B1. The time evolution of the projected mass densities for H I ($\Sigma_{\rm HI}$, left four) and H_2 ($\Sigma_{\rm H_2}$, right four) for the prograde tidal interaction model (M16).

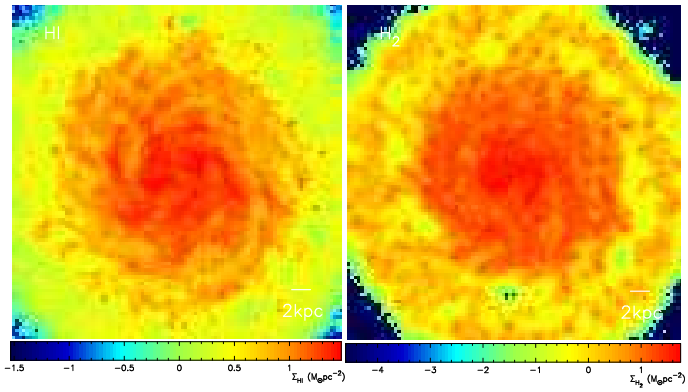

Figure B2. The final projected mass densities for H I ($\Sigma_{\rm HI}$, left) and H_2 ($\Sigma_{\rm H_2}$, right) for the high-z MW-type disk model with $f_{\rm g} = 0.55$ (M15).